

A Scalable Suspension Platform for Generating High-Density Cultures of Universal Red Blood Cells from Human Induced Pluripotent Stem Cells

Jaichandran Sivalingam,¹ Yu SuE,¹ Zhong Ri Lim,¹ Alan T.L. Lam,¹ Alison P. Lee,² Hsueh Lee Lim,² Hong Yu Chen,⁴ Hong Kee Tan,⁴ Tushar Warriar,⁴ Jing Wen Hang,⁶ Nazmi B. Nazir,⁶ Andy H.M. Tan,^{2,3} Laurent Renia,⁷ Yuin Han Loh,^{4,5} Shaul Reuveny,¹ Benoit Malleret,^{6,7} and Steve K.W. Oh^{1,*}

¹Stem Cell Bioprocessing Group, Bioprocessing Technology Institute, Agency for Science, Technology and Research, 20 Biopolis Way, Centros 06-01, Singapore 138668, Singapore

²Transcriptomics Group, Bioprocessing Technology Institute, Agency for Science, Technology and Research, Singapore 138668, Singapore

³Immunology Group, Bioprocessing Technology Institute, Agency for Science, Technology and Research, Singapore 138668, Singapore

⁴Institute of Molecular and Cellular Biology, Agency for Science, Technology and Research, Singapore 138668, Singapore

⁵Department of Biological Sciences, National University of Singapore, Singapore 117543, Singapore

⁶Department of Microbiology, Yong Loo Lin School of Medicine, National University of Singapore, Singapore 117543, Singapore

⁷Singapore Immunology Network, Agency for Science, Technology and Research, Singapore 138668, Singapore

*Correspondence: steve_oh@bti.a-star.edu.sg

<https://doi.org/10.1016/j.stemcr.2020.11.008>

SUMMARY

Universal red blood cells (RBCs) differentiated from O-negative human induced pluripotent stem cells (hiPSCs) could find applications in transfusion medicine. Given that each transfusion unit of blood requires 2 trillion RBCs, efficient bioprocesses need to be developed for large-scale *in vitro* generation of RBCs.

We have developed a scalable suspension agitation culture platform for differentiating hiPSC-microcarrier aggregates into functional RBCs and have demonstrated scalability of the process starting with 6 well plates and finally demonstrating in 500 mL spinner flasks. Differentiation of the best-performing hiPSCs generated 0.85 billion erythroblasts in 50 mL cultures with cell densities approaching 1.7×10^7 cells/mL. Functional (oxygen binding, hemoglobin characterization, membrane integrity, and fluctuations) and transcriptomics evaluations showed minimal differences between hiPSC-derived and adult-derived RBCs.

The scalable agitation suspension culture differentiation process we describe here could find applications in future large-scale production of RBCs in controlled bioreactors.

INTRODUCTION

O-negative rhesus factor D-negative (O-neg) blood, the universal donor blood type, is considered a limited and valuable source of red blood cells (RBCs) for emergency transfusion applications (Hirani et al., 2017). Anticipated supply shortages in the future due to an aging population and risks from emerging viruses and pathogens (Alter et al., 2007) have driven initiatives to develop alternate and ready sources of universal donor blood. Differentiation of RBCs from human induced pluripotent stem cells (hiPSCs) is one such approach actively being investigated. The unlimited proliferation potential of hiPSCs coupled with their potential to differentiate into hematopoietic lineages (Paes et al., 2017) has made these cells appealing as limitless sources of starting materials for generating universal RBCs. It has been postulated that as few as 10 hiPSC clones derived from patients with rare blood phenotypes would be sufficient to cover the necessary blood types for 99% of the population with recurrent transfusion needs (Peyrard et al., 2011).

Each transfusion unit of blood consists of 2 trillion RBCs. *In vitro* derivation of such large numbers of RBCs requires overcoming a few unmet challenges. First is the lack of efficient bioprocesses that can be scaled up from laboratory to

industrial scale for RBC manufacture. Although several groups have shown the potential for efficient differentiation of hiPSCs toward RBCs (Dorn et al., 2015; Mao et al., 2016; Olivier et al., 2016), most of these may not be favorable for clinical development, either due to the use of undefined or xenogenic components or due to the lack of scalability of the process. Other groups have also immortalized adult erythroblasts to produce RBCs (Trakarnsanga et al., 2017; Kurita et al., 2013; Hirose et al., 2013). Yet a second challenge that needs to be overcome is the lack of cost-effective means to achieve ultra-high-density cultures of RBCs. Given that each unit of blood requires 2×10^{12} RBCs, one would have to achieve cell densities of at least 1×10^8 cells/mL in order to generate the desired cell numbers in a minimal medium volume. Thus far, the highest reported cell density for RBC culture appears to be in the range of 1×10^7 cells/mL (Ying Wang et al., 2016).

Development of a scalable process that can eventually be transferred to large-scale stirred bioreactors would require the entire process to be performed in continuous agitation suspension culture. We have previously described means to scale up the pluripotent expansion stage by culturing hiPSCs on Laminin-521 (LN-521)-coated microcarriers (MCs) (Lam et al., 2016; Sivalingam et al., 2018). We have also shown that hiPSC-MC aggregates in suspension

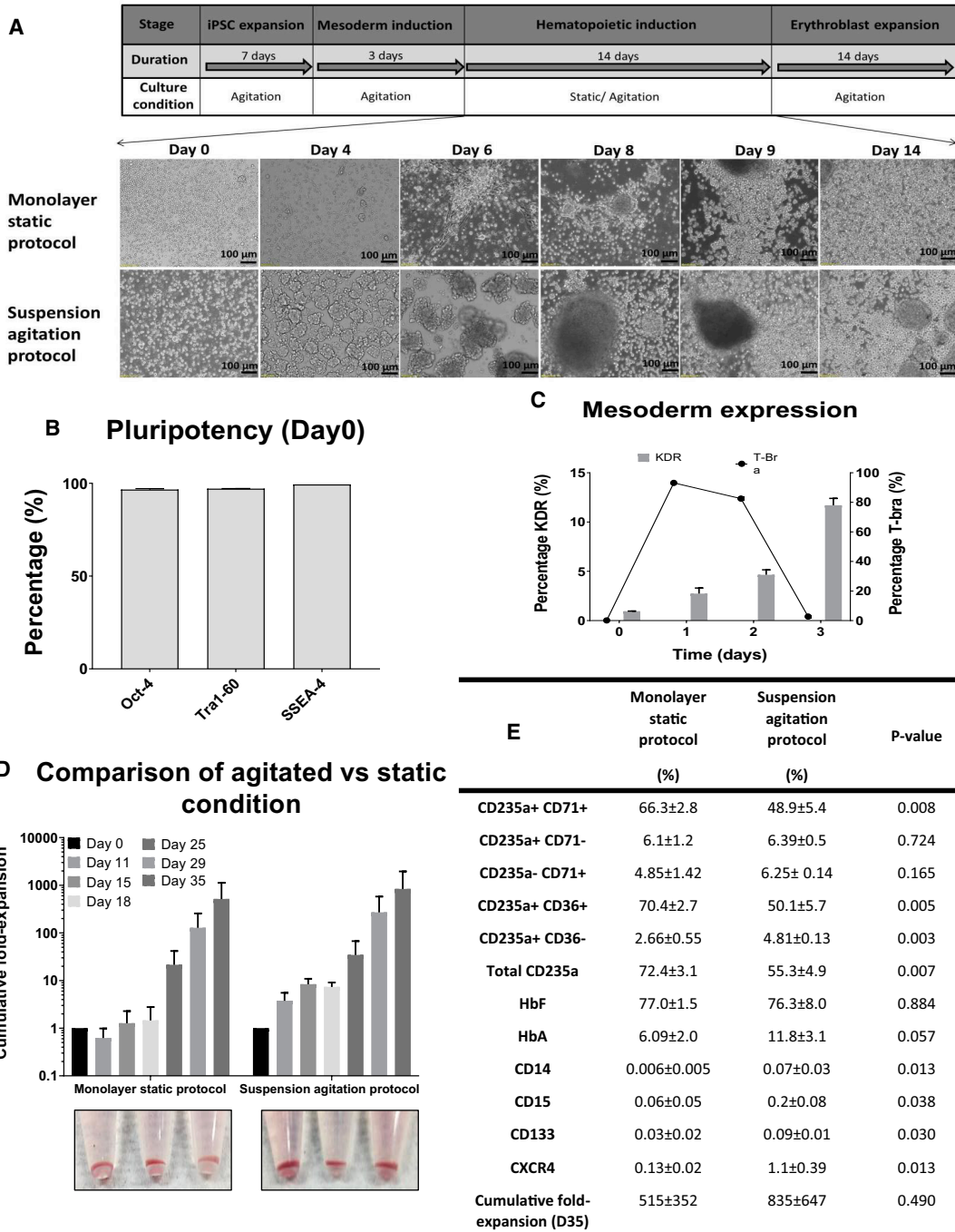


Figure 1. Development of Agitation Suspension Culture Differentiation of 0-Neg hiPSCs

(A–C) (A) Schematic of differentiation process from hiPSC to erythroblast stage. Bright-field images of cells from an 0-neg hiPSC line, D5, undergoing hematopoietic differentiation in tissue culture plates under static conditions (monolayer static protocol) or in 6 well ULA plates under continuous agitation (suspension agitation protocol) from day 0 to 14 of the hematopoietic induction stage. Flow cytometry evaluation of (B) pluripotency markers following 7 days of agitation expansion in 6 well ULA plates and (C) T-Bra and KDR cell populations during mesoderm differentiation.

(D) Cumulative fold expansion of total viable cells following differentiation using monolayer static protocol or suspension agitation protocol and corresponding hemoglobinized cell pellets observed at day 35 of differentiation. There is no significant difference in expansion fold between static and agitated conditions, $p > 0.05$.

(legend continued on next page)



culture can efficiently differentiate into T-Bra⁺ and KDR⁺ mesodermal cells (Sivalingam et al., 2018), demonstrating that hiPSC-MC aggregates could differentiate as embryoid bodies (EBs) in a scalable manner.

The current study was undertaken to develop an agitation suspension culture bioprocess for differentiation of hiPSCs to erythroid cells with prospects of transferring the process to larger-scale controlled bioreactors for future manufacture of RBCs. Using process optimization, we show that hiPSC-MC aggregates can be efficiently differentiated into mature and functional RBCs. We demonstrate the scalability of the process starting from 6 well plates all the way to 500 mL spinner flasks. We show that it is possible to differentiate hiPSC-MC aggregates into high-density cultures of erythroid cells approaching concentrations of 1.7×10^7 cells/mL in spinner flasks. More importantly, we show that functional and transcriptomics evaluation revealed minimal differences between hiPSC-derived RBCs and adult derived RBCs. The scalable agitation suspension culture differentiation process we describe could serve as a platform for developing large-scale blood differentiation processes in controlled bioreactors.

RESULTS

Continuous Agitation Suspension Culture Differentiation of hiPSC-MC Aggregates in 6 Well-ULA Plates

To develop a continuous agitation suspension culture differentiation platform, we first evaluated whether an hiPSC line expanded under agitation on MC during the pluripotent expansion and mesoderm stages could be further differentiated through the hematopoietic and erythroid induction stages under continuous agitation in suspension culture in 6 well ULA plates (suspension agitation protocol). A control experiment was performed whereby the hematopoietic induction stage was achieved on normal tissue culture plates under static conditions (monolayer static protocol) (Figure 1A). An O-neg hiPSC line, D5, was used for both of these experiments. hiPSC-MC aggregates maintained high levels of pluripotency (>98% Oct-4, Tra1-60, and SSEA-4 positive by fluorescence-activated cell sorting [FACS]) following 7 days of expansion under continuous agitation (Figure 1B). Following hematopoietic mesoderm induction for 3 days under agitation, high levels of the primitive streak/early mesoderm marker T-bra (>83%) were observed at day 1 post differentiation. KDR expression

($12 \pm 4.9\%$) was enriched by day 3 of differentiation (Figure 1C). Single cells derived by enzymatically detaching cells from MCs were seeded into either 6 well tissue culture plates (monolayer static protocol) or ULA plates (suspension agitation protocol) for hematopoietic induction. In tissue culture plates, seeded cells initially attached and expanded as adherent hemogenic endothelial cells (days 4–9) that subsequently gave rise to suspension culture hematopoietic cells with great proliferation observed by day 14 post seeding. In ULA plates, seeded single cells initially formed small clusters (150–200 μm in diameter) in suspension by day 4. Single cells were subsequently observed to emerge from these small clusters followed by expansion from day 8 to 14. Following induction of erythroid differentiation (day 14–35), extensive expansion of single suspension cells was noted, with day 35 cumulative fold expansion of continuous agitation (suspension agitation protocol: 835 ± 647) being comparable ($p > 0.05$) to static (monolayer static protocol: 515 ± 352) (Figure 1D). Both continuous agitation and static culture differentiation protocols resulted in formation of hemoglobinized erythroid cells with $55.3 \pm 4.9\%$ and $72.4 \pm 3.1\%$ expressing the CD235a erythroid marker, respectively (Figures 1D and 1E). Erythroid cells mainly expressed fetal hemoglobin, although adult hemoglobin expression at a lower level was also noted (Figure 1E).

Interestingly, in the agitation condition, extensive expansion of single cells in suspension from day 8 to 14 was observed only after the formation of cell clusters/aggregates in suspension culture (Figure S2A). Co-expression of CD34/CD144/CD31 and CD43 by FACS (Figure S2B) and immunofluorescence imaging (CD34/CD144 co-staining) (Figure S2C) established the presence of hemogenic endothelial cells (Angelos et al., 2018) (CD34⁺ CD144⁺ CD31⁺ or CD43⁺) within these cell aggregates. In contrast, single cells obtained from day 5 of differentiation did not express markers of hemogenic endothelial populations but differentiated further into CD34/CD45-expressing primitive hematopoietic progenitors (Figure S2B).

To establish if the expanding cells in suspension culture were derived from differentiation of the hemogenic endothelial cell aggregates or from primitive hematopoietic progenitors already present in suspension, we separated out the “hemogenic endothelial cell aggregates” from single cells by sieving through 40 μm sieves on day 5 of differentiation and proceeded to differentiate these different cell populations (Figure S2A). The control group was differentiated without any additional sieving (mixture of aggregates

(E) Table summarizing FACS characterization of differentiated cells from day 35 of differentiation. Percentages of erythroid-specific markers CD235a, CD71, and CD36 and fetal/adult hemoglobin expression as well as markers for myelomonocytic cells (CD14, CD15) and hematopoietic stem cells (CD133, CXCR4) are shown together with cumulative fold expansion on day 35. All data represent the mean \pm SD with at least three independent replicates. Representative experiment shown.

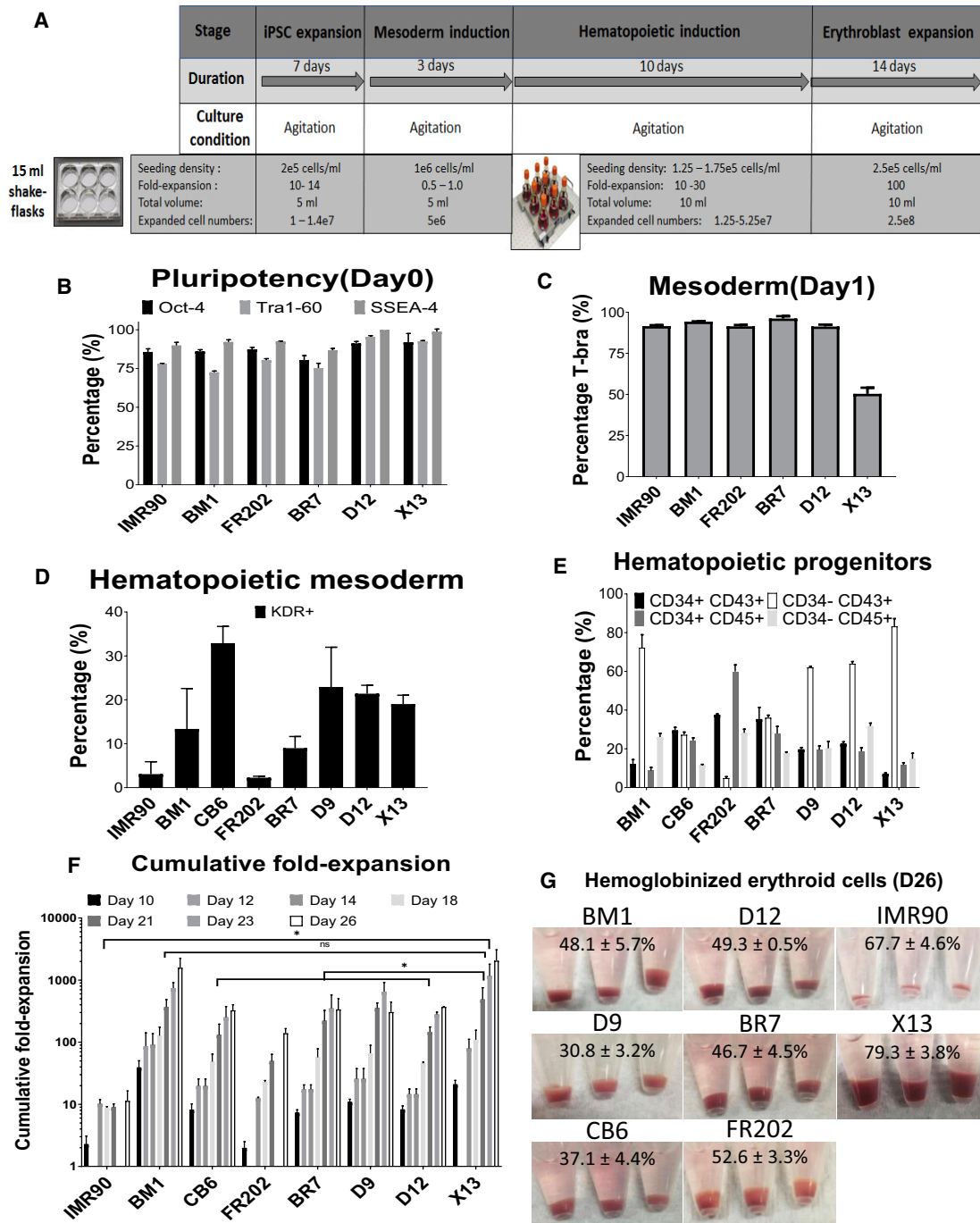


Figure 2. Agitation Suspension Culture Differentiation of Multiple hiPSC Lines in Shaker Flasks

(A–F) (A) Schematic showing initial expansion of cell-MC aggregates in 6 well ULA plates during iPSC expansion and mesoderm induction stages. Subsequent stages of differentiation were achieved in 50 mL shaker flasks under continuous agitation. FACS evaluation of (B) pluripotency markers (insufficient samples for CB6 and D9), (C) mesoderm/primitive-streak marker (T-bra) (day 1 of differentiation; insufficient samples for CB6 and D9), (D) hematopoietic-fated mesoderm markers (KDR⁺) (day 3 of differentiation), and (E) hematopoietic progenitor markers (CD34⁺CD43⁺, CD34⁺CD45⁺)/committed hematopoietic cells (CD34⁻CD43⁺, CD34⁻CD45⁺) (day 12 of differentiation) for multiple hiPSC lines (insufficient samples for IMR90).

(legend continued on next page)



and single cells). Interestingly, the majority of expansion was observed in the groups that had the hemogenic endothelial cell aggregates (control group I, no sieving, 30.2 ± 4.3 -fold expansion; group II, sieved cell aggregates, 28.7 ± 21.4 -fold expansion on day 21) rather than single cells (group III, sieved non-aggregated single cells, 1.6 ± 1.5 -fold expansion). Erythroid differentiation from sieved hemogenic endothelial aggregates (aggregated population) was similar to that of the control group (no sieving), while differentiation of the sieved single cells (non-aggregated population) failed to result in erythroid differentiation (Figure S2D). Taken together, these data suggest that the hematopoietic differentiation reported in our continuous suspension agitation protocol was via differentiation from hemogenic endothelial cell clusters rather than from expansion of primitive hematopoietic progenitor cells.

Differentiation of Multiple hiPSC Lines in 50 mL Shaker Flasks Using Continuous Agitation Suspension Differentiation Approach

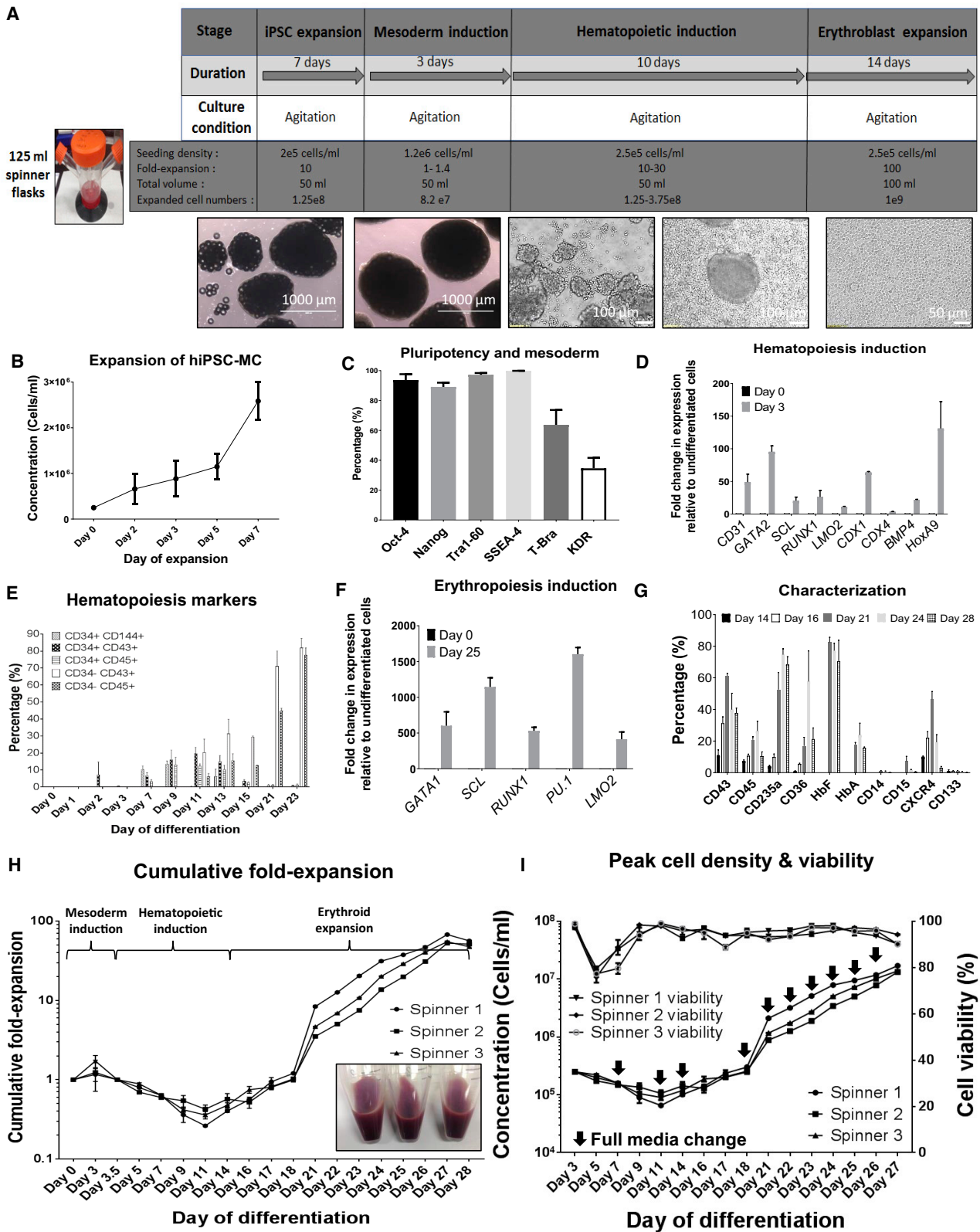
Having established that erythroid differentiation from hiPSCs can be entirely performed in suspension under continuous agitation conditions, we next proceeded to evaluate differentiation of hiPSCs derived from O-neg erythroid progenitors (D9, D12, X13, BR7) and of cord-blood-derived hiPSCs (CB6), bone-marrow-derived hiPSCs (BM1), and dermal-fibroblast-derived hiPSCs (FR202 and IMR90). For each hiPSC line, pluripotent expansion (7 days) and mesoderm differentiation (3 days) of hiPSC-MC aggregates were first established in 6 well ULA plates. After 3 days of hematopoietic mesoderm development, single cells derived following trypsinization of hiPSC-MC aggregates were further differentiated in 50 mL shaker flasks (Figure 2A). hiPSC-MC aggregates maintained their pluripotency during the expansion stage (Oct-4, 80.4%–92.0%; Tra1-60, 72.5%–95.4%; and SSEA-4, 86.8%–99.9%) (Figure 2B), differentiated into T-Bra⁺ primitive streak/mesoderm (50.4%–96.2%) on day 1 of differentiation (Figure 2C), and had evidence of hematopoietic-fated mesoderm marker KDR⁺ (3.1%–32.9%) by day 3 of differentiation (Figure 2D). Among these eight lines, the mesoderm differentiated from CB6 showed the highest KDR⁺ hematopoietic mesoderm marker, which was $32.9\% \pm 3.8\%$. By day 12 of differentiation, CD34⁺ CD45⁺ (8.8%–59.9%) and CD34⁺ CD43⁺ (7.2%–37.6%) hematopoietic progenitor cells, as well as more mature CD34⁻ CD45⁺ (11.6%–31.7%) and CD34⁻ CD43⁺ (4.9%–83.3%) hematopoietic-

committed cells, were detected (Figure 2E). CD34⁻ CD43⁺ hematopoietic-committed cells from X13 displayed the highest levels ($83.3\% \pm 6.7\%$) compared with the other seven lines (Figure 2E). Following erythroid differentiation, BM1 ($1,580 \pm 675$) and X13 ($2,049 \pm 1,019$) achieved the highest cumulative fold expansion by day 26 of differentiation (Figure 2F). All eight hiPSC lines were able to differentiate into hemoglobinized erythroblasts (Figure 2G), with CD235a⁺ expression ranging from 30.8%–79.3%. X13 hiPSC differentiated erythroblasts yielded $79.3 \pm 3.8\%$ CD235a⁺ erythroblasts, highest among the eight lines differentiated (Figure 2G). To investigate whether there was correlation between D26 CD235a⁺ erythroblast production and the different hematopoietic markers, we performed a heatmap analysis (Figure S3B). Among all the parameters, only the marker CD34⁻ CD43⁺ had an R² value of 0.486 (Figure S3A), which indicates that these different hematopoietic markers do not have a strong correlation with final RBC production.

Both fetal hemoglobin and adult hemoglobin expression was verified by immunoblotting (Figure S3C). Expression of embryonic hemoglobin (Epsilon in the figure) was detected in BM1, D12, and X13 hiPSCs, suggesting the presence of erythroid cells derived from primitive erythropoiesis. Interestingly, erythroid cells differentiated from CB6, BR7, and D9 hiPSCs had little or no embryonic hemoglobin, suggesting that these cells may have been differentiated via definitive erythropoiesis. Oxygen equilibrium profiles of erythroblasts differentiated from hiPSCs were left-shifted (p50: 12.4 to 14.7) compared with adult RBCs (p50: 20.7 ± 1.0) (Figure S3D). Following erythroblast expansion, from day 18 to 26, maximal cell concentrations ranged from 4 to 12.6×10^6 cells/mL (Figure S3E). Complete medium replenishment was critical for cell viability and expansion, especially when cell densities were high ($>8 \times 10^6$ cells/mL). For instance, at day 23, both D9 (▼) and X13 (▼) differentiated erythroblasts had high cell densities and viabilities (D9 9.64×10^6 cells/mL, $97.2 \pm 1.2\%$ viability; X13 8.63×10^6 cells/mL, $97.1 \pm 1.0\%$ viability). However, without medium renewal for 24 h, D9 erythroblast cell concentrations dropped to 7.35×10^6 cells/mL and $70.8 \pm 8.1\%$ viability (day 24), whereas with complete medium renewal, X13 erythroblasts continued to proliferate to 1.25×10^7 cells/mL and maintained a high viability of $96.5 \pm 0.7\%$ (day 26). Analysis of the conditioned medium from day 24 cultures showed that lactate and ammonia levels had spiked to 2.49 ± 0.03 g/L

(F) Cumulative fold expansion of total viable cells following differentiation of multiple human iPSC lines on shaker flasks. * $p < 0.05$ comparing X13 with other lines except for BM1.

(G) Corresponding hemoglobinized cell pellets at day 26 of differentiation with percentage of CD235a⁺ cells (determined by FACS) indicated. All data represent the mean \pm SD with at least three independent replicates. Representative experiment shown.



(legend on next page)



and 4.65 ± 0.2 mM, respectively, for D9 erythroblast cultures without medium renewal for 24 h. For X13 erythroblasts that received medium renewal on day 23, lactate and ammonia levels were significantly lower ($p < 0.05$) at 0.96 ± 0.2 g/L and 1.05 ± 0.2 mM, respectively (Figure S3F). Thus, the X13 hiPSC line was chosen as the best-performing line for erythroid cell differentiation with the highest cumulative fold expansion. High-resolution digital karyotyping performed on genomic DNA of X13 differentiated erythroid cells showed normal copy numbers (defined as between 1.6 and 2.4 copies) for all chromosomes evaluated (Figures S3G and S3H).

Scale-Up of Continuous Agitation Suspension Culture Differentiation to 125 mL Spinner Flasks

Following the demonstration that multiple hiPSC lines can be differentiated under constant agitation condition in 50 mL shaker flasks, we next chose to demonstrate scale-up of differentiation and reproducibility in 125 and 500 mL spinner flasks (Figure 3A). X13 hiPSCs, which had the best differentiation outcome in shaker flasks, were used for this study. In 125 mL spinner flasks, X13-MC aggregates achieved approximately 10-fold expansion during the pluripotent stage (Figure 3B) while maintaining pluripotency levels (Figure 3C). Upon onset of differentiation of X13 hiPSC-MC aggregates, the primitive streak/early mesoderm marker T-bra ($63.7 \pm 10\%$) and hematopoietic-fated mesoderm KDR⁺ marker ($34.6 \pm 6.9\%$) were detected at days 1 and 3 post differentiation, respectively (Figure 3C). KDR⁺ CD235a⁻, another marker indicative of definitive hematopoiesis (Sturgeon et al., 2014), was also detected on day 3 ($15.6 \pm 2\%$). Key markers and transcription factors involved in early hematopoiesis were found

to be upregulated by day 3 of differentiation (fold upregulation compared with undifferentiated cells; Figure 3D). CD34⁺ CD144⁺ hemogenic endothelial cells ($10.3 \pm 3.6\%$) were detected as early as 7 days post differentiation. CD34⁺ CD43⁺ ($19.7 \pm 6.2\%$) and CD34⁺ CD45⁺ ($12.2 \pm 2.3\%$) hematopoietic progenitors peaked at around day 11 post differentiation and continued to mature into CD34⁻ CD43⁺ ($81.9 \pm 9.5\%$) and CD34⁻ CD45⁺ ($77.8 \pm 7.1\%$)-committed hematopoietic cells until day 23 post differentiation (Figure 3E). During erythroid differentiation, key markers and transcription factors associated with erythropoiesis were upregulated (Figure 3F). A significant increase in CD235a⁺ erythroid cells was noted starting from day 16 ($9.9 \pm 1.9\%$) to day 24 ($74.7 \pm 3.6\%$) of differentiation (Figure 3G). Day 24 differentiated erythroblasts had high levels of HbF ($77.1 \pm 7.5\%$) and lower levels of HbA ($23.8 \pm 7.4\%$). By day 28 of differentiation, the cultures had very few hematopoietic stem cells (<3% CXCR4 and <0.5% CD133) and a negligible amount of (<1%) myelomonocytic cells (CD14/CD15) (Figure 3G and Table 1). X13 hiPSC-MC aggregates expanded 1.1- to 1.7-fold during mesoderm induction. Following single-cell seeding after 3 days of mesoderm induction, from day 5 to day 11, no expansion was observed, possibly due to the seeded single cells forming hemogenic endothelial cell aggregates. From day 11 onward, cell expansion was noted, with exponential increase in cell numbers observed during the erythroid expansion stage (day 18 onward). All three spinner cultures yielded hemoglobinized erythroid cells with an average cumulative fold expansion of 58.6 ± 8.1 -fold on day 27 of differentiation (Figure 3H). With complete medium replenishment during the erythroblast expansion stage, we were able to achieve mean peak cell densities of

Figure 3. Scale-Up of Differentiation of X13 hiPSC in 125 mL Spinner Flasks

- (A) Schematic of suspension culture continuous agitation differentiation process from hiPSC to erythroblast stage in 125 mL spinner flasks. Corresponding images of cell aggregates/cells during differentiation are shown below.
- (B and C) (B) Concentration of viable cells during pluripotent expansion stage. (C) Flow cytometry evaluation of pluripotency markers (Oct-4, Tra1-60, SSEA-4), mesoderm/primitive streak marker (T-bra), and hematopoietic-fated mesoderm marker (KDR⁺) (representative experiment shown).
- (D) RT-PCR quantified fold expression of early markers (*GAPDH* normalized) involved in hematopoietic induction at day 3 of differentiation.
- (E) Time course of marker expression for hemogenic endothelial cells (CD34⁺ CD144⁺), hematopoietic progenitor markers (CD34⁺ CD43⁺; CD34⁺ CD45⁺), and pan-hematopoietic markers (CD34⁻ CD43⁺; CD34⁻ CD45⁺) during the course of differentiation.
- (F) RT-PCR quantified fold expression of markers upregulated during erythropoiesis at day 25 of differentiation relative to undifferentiated cells.
- (G) Time course of marker expression (determined by FACS) during the differentiation process from day 14 to 28. Data in (B, D, E, F, G) represent the mean \pm SD with at least three independent replicates. Representative experiment shown.
- (H) Cumulative fold expansion of cells during pluripotent expansion (day -8 to day 0), mesoderm induction (day 0 to day 3), hematopoietic induction (day 5 to day 14), and erythroid expansion (day 15 to day 28) stages, in three independent spinner flasks ($p > 0.05$ indicates three independent spinner flasks are equivalent). Corresponding hemoglobinized cell pellets at day 28 of differentiation are shown.
- (I) Concentration of viable cells and corresponding viability in three independent spinner flask experiments during differentiation are shown. Black arrows indicate complete medium change. Statistical tests were performed on the pooled data from at least three independent replicates.

**Table 1. Expression Profile of X13 hiPSC-Derived Erythroblasts from Spinner Culture Differentiation**

Expression Profile	Marker	Spinner 1	Spinner 2	Spinner 3	Mean ± SD
Erythroid	CD235a	63.5	73.5	68.1	68.4 ± 5.0
Early erythroid	CD235a ⁺ CD71 ⁺	44.3	58.5	51.4	51.4 ± 7.1
Late erythroid	CD235a ⁺ CD71 ⁻	19.2	15	16.7	16.9 ± 2.1
Thrombospondin receptor	CD36	16.8	29.4	17.5	21.2 ± 7.1
Hematopoietic progenitor	CD45	13.1	7.6	10.5	10.4 ± 2.8
Hematopoietic progenitor	CD43	40.7	34.3	37.8	37.6 ± 3.3
Hematopoietic stem cell	CXCR4	3.74	3.21	1.84	2.9 ± 1.0
Hematopoietic stem cell	CD133	0.17	0.09	0.08	0.12 ± 0.05
Myelomonocytic cell	CD15	0.47	0.58	0.51	0.5 ± 0.05
Myelomonocytic cell	CD14	0.17	0.12	0.12	0.14 ± 0.03
Fetal hemoglobin	HbF	59.6	85.4	66.3	70.4 ± 13.3
Adult hemoglobin	HbA	16.3	15.2	15.3	15.6 ± 0.69

$1.47 \times 10^7 \pm 2.04 \times 10^6$ cells/mL with $91.4 \pm 2.4\%$ viability (Figure 3I), generating an average of 7.35×10^8 cells with a total medium usage of 575 mL from start to end of differentiation. Metabolic profiles from Table 2 suggest that at cell densities above 1×10^7 cells/mL, lactate levels could reach inhibitory levels >15 mM or 1.36 g/L (Bayley et al., 2018; Hassell et al., 1991) within 1.5 days without medium replenishment. However, glucose consumption was found to be non-limiting at these cell densities.

The aforementioned spinner flask differentiation approach was applied to another hiPSC line, FR202. Figure S4A shows the FR202 hiPSCs expanded and differentiated into the mesoderm lineage on MCs in spinner flasks under continuous agitation. Following hematopoietic induction and erythroid differentiation in 125 mL spinner flasks, cells successfully formed hemoglobinized erythroblasts. Like X13 hiPSCs, expression of the mesoderm marker T-Bra, hematopoietic mesoderm marker KDR⁺, and hematopoietic markers CD34⁺ CD43⁺ and CD34⁺ CD45⁺ on cells was noted during the mesoderm and hematopoietic induction stages, respectively (Figure S4B). Erythroid cells differentiated from FR202 hiPSCs were able to reach a cell density between 5.44×10^6 and 9.88×10^6 cells/mL by day 29 of differentiation (Figure S4C), achieving a cumulative fold expansion between 206- and 805-fold (Figure S4D) and a total yield of $3.3\text{--}5.9 \times 10^8$ erythroid cells in a final volume of 60 mL. Differentiated cells were 50% CD235a⁺ erythroblasts, which had high expression of fetal hemoglobin (Figure S4E). As with X13 differentiated erythroblasts, oxygen equilibration curves were left-shifted (p50: 10.5) compared with adult RBCs (p50: 16.3) (Figure S4F). We were able to scale up

the erythroid differentiation process to 500 mL spinner flasks, generating approximately 1.6×10^9 erythroid cells in 200 mL volumes at densities of $8.2 \times 10^6 \pm 5.9 \times 10^5$ cells/mL.

Transcriptome Analysis of hiPSC Erythroblasts versus Adult Erythroblasts

Having achieved scale-up of erythroid differentiation from hiPSCs, it is important to determine whether erythroblasts thus generated are similar in terms of gene expression to counterparts differentiated from adult peripheral blood cells. To this end, we performed microarray-based transcriptome profiling of D24 erythroblasts derived from X13 hiPSCs and the adult peripheral blood CD34⁺ cells from the same donor (X13). Representative Giemsa staining of X13 iPSC-derived and adult blood-differentiated erythroblasts showed similar morphologies, reflecting mainly erythroblast cells, and a portion of more mature erythroblasts with condensed nuclei and reduced cell size (Figure 4A). Average linkage clustering of expressed genes ($n = 10,342$) and volcano plots revealed minimal changes in gene expression across two groups (Figure 4B). Comparison of erythroblasts differentiated from X13 hiPSCs with those differentiated from adult CD34 cells identified 119 differentially expressed genes (DEGs) (73 upregulated; 46 downregulated) (Figure 4C). We found that most of them, 64 of 73 upregulated DEGs (Figure S5A) and 40 of 46 downregulated DEGs (Figure S5B), had less than 10-fold change in expression. Pathway mapping of DEGs showed that only 3 of 73 upregulated genes mapped significantly to a single identified pathway (metabolism of xenobiotics by cytochrome p450; $p = 1.7 \times 10^{-2}$) (Figure S5C) and 9 of



Table 2. Peak Cell Density, Glucose Consumption, and Metabolite Production in Deriving Erythroblasts at Day 27 of Differentiation

Day 27	Spinner 1	Spinner 2	Spinner 3
Concentration (cells/mL)	$1.7 \times 10^7 \pm 5.2 \times 10^5$	$1.32 \times 10^7 \pm 5.5 \times 10^5$	$1.38 \times 10^7 \pm 5.5 \times 10^5$
Total cells/50 mL	$8.5 \times 10^8 \pm 2.6 \times 10^7$	$6.6 \times 10^8 \pm 2.7 \times 10^7$	$6.9 \times 10^8 \pm 2.7 \times 10^7$
Total medium used (mL)	575	575	575
Lactate production (mg/L/per 24 h/ million cells)	1.76	1.73	1.81
Ammonia production (mM/per 24 h/ million cells)	0.0016	0.0014	0.0018
Glucose consumption (mg/L/per 24 h/ million cells)	1.7	1.1	1.3

46 downregulated genes mapped significantly to three different pathways (tuberculosis, hematopoietic cell lineage, and nitrogen metabolism) (Figure S5D). Gene ontology classification of DEGs revealed that a majority were categorized as being involved in biological regulation (upregulated 17%, downregulated 22%) and metabolic processes (upregulated 22%, downregulated 18%) (Figures S5E and S5F). To ascertain if erythroblasts differentiated from hiPSCs versus adult CD34⁺ cells differed in certain biological processes, we next focused on genes involved in growth (cell-cell signaling, cell cycle, cell proliferation, mitochondria), maturation (apoptosis, autophagy), and functional characteristics (erythrocyte membrane, cytoskeleton, hemoglobin) (Figure 4D). Comparison of DEGs between hiPSCs and adult erythroid cells revealed significant differences in expression of only a small number of genes involved in apoptosis, cytoskeleton, cell proliferation, cell signaling, mitochondria, cell cycle, and hemoglobin (Figure 4C). qRT-PCR was used to verify changes in gene expression of selected DEGs (14 of 28 DEGs) from the above-mentioned categories, and we observed concordance between qRT-PCR and microarray results for adult versus hiPSC erythroid cells (Figure S5G). Previous transcriptome (Merryweather-Clarke et al., 2016) and proteomic (Wilson et al., 2016) studies highlighted differences in the expression of key erythropoiesis and other genes between hiPSCs and adult erythroblasts. These included genes involved in heme biosynthesis, erythropoiesis, autophagy, cytoskeleton, and biological regulation by intracellular enzymes. Our microarray analysis revealed significant differences (fold change ≥ 1.5 ; $p < 0.05$) in the expression

of only two of the previously identified genes (*ARID3A* and *BCL11A*) between hiPSCs and adult erythroblasts (Table S1 and Figure S5H), suggesting that erythroblasts generated from hiPSCs using our scale-up method are substantially more similar in gene expression to adult erythroblasts compared with what others have previously accomplished.

Functional Evaluation and Terminal Maturation of Differentiated Erythroblasts

Having demonstrated differentiation of hiPSCs toward high-density cultures of erythroid cells, we next performed functional validation of the erythroblasts. Expression of hemoglobin protein subtypes was confirmed by immunoblots (Figures 5A and S6A). Erythroblasts differentiated from hiPSCs in spinner flasks (spinner X13) expressed alpha, beta, and gamma globins and had low-level expression of the epsilon hemoglobin subtype. On the other hand, adult RBCs from peripheral blood expressed only alpha and beta hemoglobin, consistent with the expression pattern of adult hemoglobin. Consistent with the expression of gamma hemoglobin, which has higher affinity for oxygen, the P_{50} values for oxygen equilibration curves of erythroblasts differentiated from hiPSCs in spinner flasks (P_{50} : 12.1–12.7) were significantly lower than those of adult RBCs (P_{50} : 17.9) (Figure 5B). A critical process in erythroid development is the terminal maturation of erythroblasts into enucleated erythrocytes. Using qRT-PCR we first evaluated the expression of genes involved in hemoglobin switching (HbF to HbA) and the terminal maturation process. Following terminal maturation, *KLF1* (1.8-fold), a key transcription factor necessary for HbF to HbA switching, and *BCL11A* (variants *BCL11A-L*, 4.1-fold, and *BCL11A-XL*, 31.7-fold), another transcription factor implicated in repression of HbF (Trakarnsanga et al., 2014), were found to be expressed at significantly higher levels in hiPSC-derived erythroid cells compared with RBCs differentiated from adult CD34 cells (adult RBC) (Figure 5C). *GATA-1*, a master regulator of erythropoiesis, was 2.9-fold higher, while *GATA-2* was 1.6-fold lower compared with adult RBCs, consistent with the expected decline in *GATA-2* levels during the onset of terminal maturation (Leonard et al., 1993).

Reduction in cell size was noted during the course of differentiation, with cells having a mean diameter of $12.6 \pm 0.14 \mu\text{m}$ at the start of differentiation and $7.42 \pm 0.16 \mu\text{m}$ at the end of erythroblast expansion (day 28) and finally $6.28 \pm 0.07 \mu\text{m}$ following 11 days of terminal maturation (day 39) (Figure 5D).

To demonstrate the feasibility of scale-up of erythroblasts co-cultured with stromal cell lines, we show that a murine stromal cell line, OP9, can be effectively grown on MCs under agitation. Intriguingly, in the absence of OP9

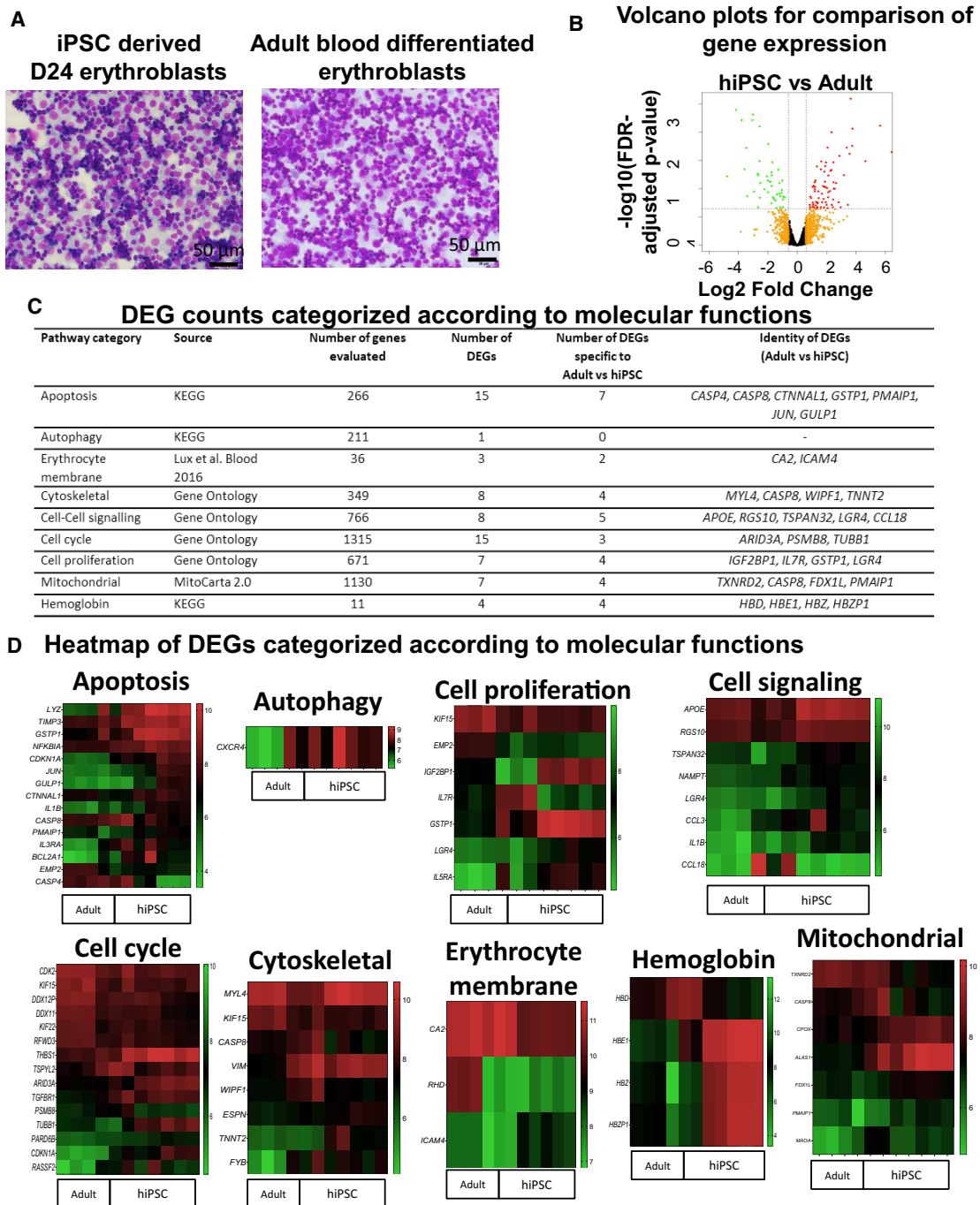


Figure 4. Transcriptome Comparison of Erythroid Cells Differentiated from X13 hiPSC and X13 Donor Adult Peripheral Blood

(A) Representative Giemsa staining of X13 iPSC-derived and adult CD34 blood-differentiated erythroblasts for transcriptome study. (B) Volcano plots for comparison of gene expression (log₂ fold change) between the day 24 erythroid cells differentiated from hiPSC (n = 5 samples) and the adult CD34 cells (n = 3 samples). Red and green dots indicate significantly up- and downregulated genes, respectively (absolute fold change ≥ 1.5 and false discovery rate [FDR]-adjusted p < 0.05), while orange dots denote the remaining genes that have absolute fold change ≤ 1.5. The dotted lines indicate the fold change and FDR-adjusted p value thresholds that were applied.

(legend continued on next page)



co-culture, X13 hiPSC-derived erythroblasts (no OP9) succumbed to massive cell death and apoptosis, whereas with OP9 co-culture (as a monolayer or on MC under agitation) efficient enucleation and reduced apoptosis were observed after 21 days of maturation (Figure 5E). In three independent experiments, the enucleation efficiencies (DRAQ5⁻, Annexin V⁻ population) of X13 hiPSC-differentiated erythroblasts after 21 days of maturation were noted to be low for conditions without OP9 co-culture (no OP9, 6.27%–6.42%) and were much higher in the presence of OP9 co-culture either as a monolayer (2D OP9, 34.1%–42.2%) or as 3D-MC with agitation (3D OP9-MC, 18.1%–59.3%).

Enucleated RBCs could effectively be enriched (Figure 5F) by passing through non-woven fabric (NWF) filters or leukocyte reduction filters (Pall). Figure 5F shows bright-field and scanning electron microscopy (SEM) images of enucleated RBCs having a biconcave appearance. Giemsa staining shows that adult blood-derived RBCs measure less than 10 μm in diameter, whereas *in vitro*-differentiated RBCs from adult and hiPSCs are slightly larger than 10 μm in diameter (Figure S6B). Quantitative phase imaging and refractive index tomography were used to compare cellular volume, surface area, sphericity, hemoglobin content, hemoglobin concentration, and dynamic membrane fluctuations of purified populations of enucleated RBCs (Figures 5G and S6C). Cellular volume and surface area were found to be significantly greater ($p < 0.0001$) in both *in vitro*-differentiated cells (adult CD34 and hiPSC) compared with adult blood. hiPSC-differentiated cells generally had a higher cellular volume and surface area (Figures 5G i and 5G ii), possibly due to a higher proportion of immature reticulocytes compared with adult CD34 and adult blood-derived cells (33.6%, Figure S7A). Adult blood- and adult CD34-differentiated RBCs and hiPSC RBCs differed in their sphericity index (ranging from 0.55 to 0.75), with hiPSC RBCs displaying the least discoid profile (sphericity of 0.75), again possibly due to a greater proportion of reticulocyte cells (Figure 5G iii). Comparison of hemoglobin concentrations showed that adult blood generally had slightly higher levels compared with adult CD34- and hiPSC-differentiated RBCs (Figure S6C i). On the other hand, measurement of mean Hb content showed that hiPSC-differentiated RBCs, due to their larger cellular volume, had significantly higher Hb content compared with adult blood and adult CD34 RBCs (Figure S6C ii). Last, dynamic membrane fluctuations were measured as an indication of membrane de-

formability of the RBCs. The dynamic membrane fluctuations of *in vitro*-differentiated RBCs from adult CD34 (145.2 nm) were found to be significantly higher than those of adult blood (55.7 nm) and hiPSC (71.4 nm) (Figure 5G iv). Three-dimensional tomography imaging of adult blood-, adult CD34-, and hiPSC-differentiated RBCs identified cells with discoid appearance (Figure S7B).

Finally, high-resolution electron microscopy imaging of enucleated RBCs derived from *in vitro* differentiation of hiPSCs and adult CD34 cells revealed that RBCs from both groups had good surface morphology (Figure S7C).

DISCUSSION

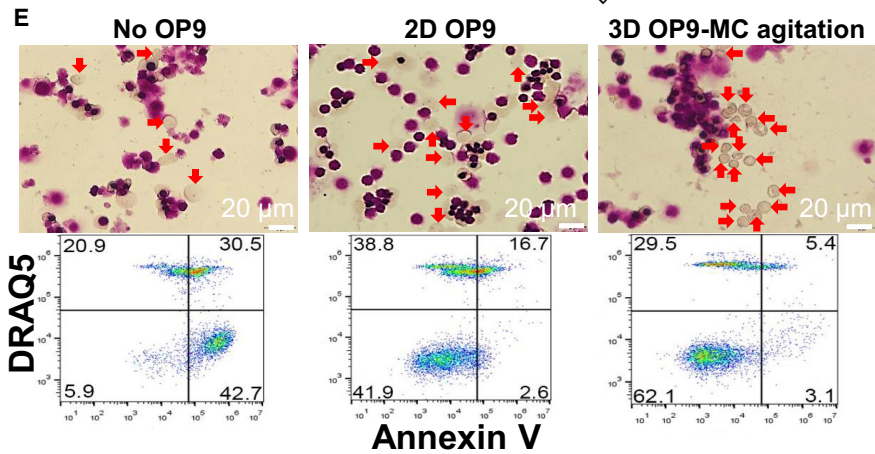
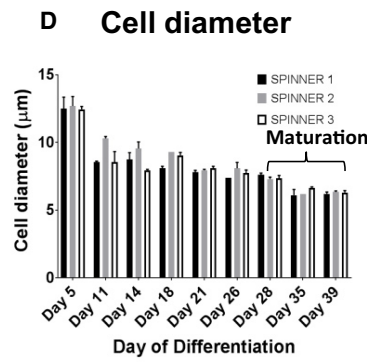
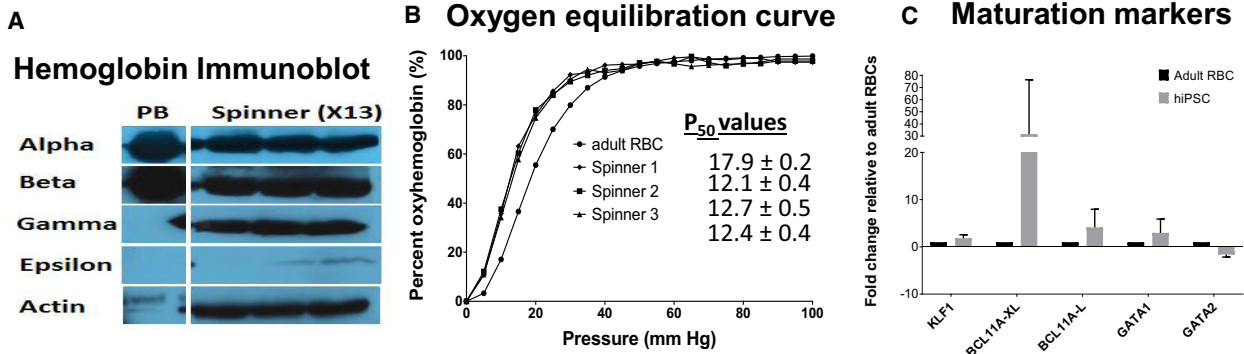
hiPSCs have been investigated as a potentially limitless source of cells for generating RBCs (Dorn et al., 2015; Mao et al., 2016; Olivier et al., 2016; Sivalingam et al., 2018). However, to date, scale-up of the differentiation process starting from the hiPSC stage to the EB stage and subsequent hematopoietic and erythroblast stages have not been clearly demonstrated.

Olivier et al. (Olivier et al., 2016) had previously described an EB-based differentiation process that allowed for generating 50,000–200,000 erythroid cells per hiPSC seeded. Although the process allowed for generation of large numbers of erythroid cells, it required the initial differentiation of EB-differentiated cells as a monolayer in tissue culture flasks, thereby making the process restrictive to scale-up.

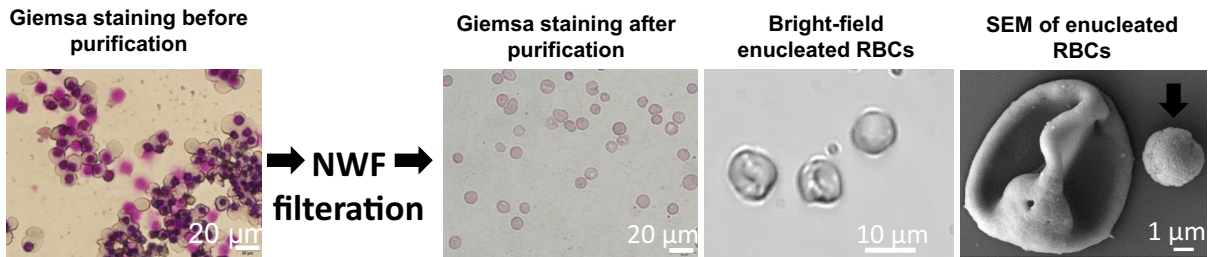
In this work, by modifying the protocol described by Olivier et al. (Olivier et al., 2016) and combining with our previously reported hiPSC-MC differentiation protocol (Sivalingam et al., 2018), we were able to demonstrate an entirely suspension-culture-based differentiation process performed under continuous agitation. We successfully scaled up the differentiation process, starting from 6 well ULA plates to shaker flasks and finally demonstrating in stirred spinner flasks as a prelude to scaling up to controlled stirred-tank bioreactors. Using the MC-hiPSC aggregates has an added advantage of generating consistent and evenly sized MC-EBs, which have been demonstrated to be scalable in suspension culture platforms (Lam et al., 2016; Sivalingam et al., 2018). Furthermore, in our spinner culture differentiation platform, by keeping the levels of lactate in culture below their inhibitory threshold, we show peak cell densities that are at least 4-fold higher

(C) Table showing number of DEGs belonging to the different categories. Genes evaluated for each category were derived from the indicated sources.

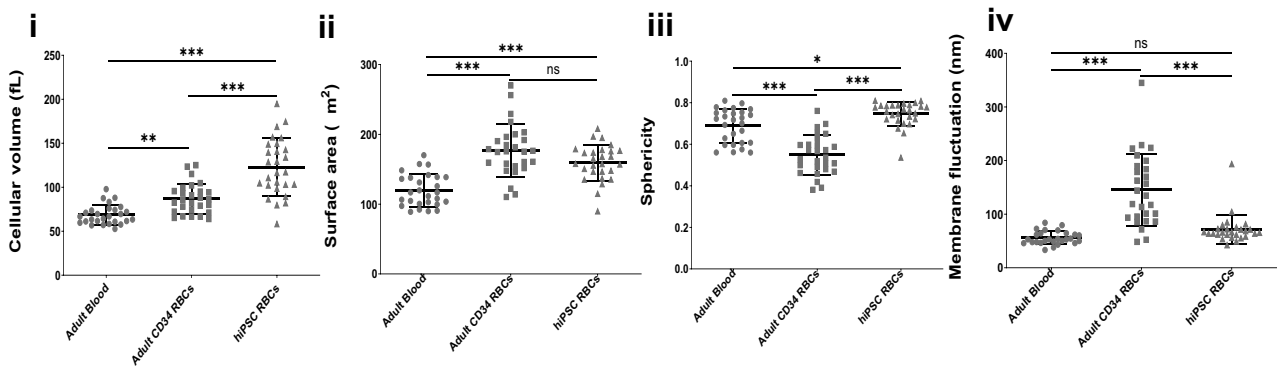
(D) Heatmaps (normalized expression signal intensity) of significant DEGs categorized according to molecular functions (apoptosis, autophagy, cytoskeletal, cell proliferation, cell signaling, cell cycle, erythrocyte membrane, mitochondrial, and hemoglobin) for comparison.



F Enrichment of terminally matured RBCs



G Quantitative Phase Imaging measurements of enucleated RBCs



(legend on next page)



(1.7×10^7 cells/mL) than the 4×10^6 cells/mL that was reported previously (Ying Wang et al., 2016). To generate one transfusion unit of RBCs (1×10^{12} cells) in a minimum operation volume of a 20 L bioreactor, one would ideally have to reach cell densities exceeding 1×10^8 cells/mL. Data suggest that even at erythroid cell concentrations of 1.7×10^7 cells/mL, lactate (inhibitory level >15 mM) and ammonia (inhibitory level >4 mM) can reach inhibitory levels (Bayley et al., 2018) in less than 1.5 days without medium replenishment. As such, further process refinements such as a dilution feeding strategy (Zhang et al., 2017) or perfusion strategy (Allenby et al., 2018) may be necessary in order to replenish depleted cytokines/growth factors/nutrients, as well as preventing the accumulation of culture metabolites from reaching inhibitory levels in order to allow for cell densities exceeding 1×10^8 cells/mL to be achieved.

In performing high-density cultures, it is pertinent to demonstrate that the final cell product is healthy and functional. In this study, high-resolution electron microscopy imaging and quantitative phase imaging provided additional evidence that hiPSC-derived RBCs (in comparison with adult-derived RBCs) do have good membrane morphology and similar dynamic membrane fluctuation profiles (Kim et al., 2018) indicative of their membrane deformability capabilities, which would be important for passing through narrow capillaries in the human body.

Comparison of the gene expression of adult and hiPSC erythroblasts identified $<1.2\%$ of expressed genes (119 of 10,342) with expression fold change greater than or equal

to 1.5-fold. None of these DEGs mapped significantly to erythroid cell-specific signaling pathways as evaluated by DAVID pathway mapping analysis. Further query of these 119 DEGs against a database of genes directing important molecular functions of erythroid cells (4,755 genes) such as apoptosis, autophagy, erythrocyte membrane, cytoskeleton, cell-cell signaling, cell cycle, cell proliferation, mitochondrial, and hemoglobin biogenesis produced only 33 hits, suggesting a high degree of similarity between hiPSC- and adult-derived erythroblasts. In terms of the erythropoiesis induction-related genes examined in Figure 3F, there were no significant differences between the adult- and the hiPSC-derived erythroblasts (Figure S4G).

A potential issue with the use of hiPSC-derived erythroid cells for transfusion applications would be the lack of reduced adult beta hemoglobin expression relative to adult-derived RBCs. By immunoblot analysis, we show that the hiPSC-differentiated erythroid cells do express both adult and fetal hemoglobin, with little or no embryonic hemoglobin, although the levels of adult beta hemoglobin from hiPSC-erythroid cells are significantly less compared with adult RBCs. Differences observed in hemoglobin expression could lead to altered affinity of the RBCs for oxygen binding and release. With regard to this, it should be pointed out that individuals with hereditary persistence of fetal hemoglobin who have high levels of gamma fetal hemoglobin (up to 30% of total hemoglobin) are asymptomatic and pathologically normal (Christaki et al., 2019). Previous studies have shown that overexpression of *KLF1* and *BCL11a* could bring about hemoglobin

Figure 5. Terminal Maturation of X13 hiPSC-Derived Erythroblasts from Spinner Differentiation

(A) Cell lysates from peripheral blood (PB) and X13 hiPSC-derived erythroblasts from spinner differentiation (day 27 post differentiation) were immunoblotted with antibodies specific to alpha, beta, gamma, and epsilon human hemoglobin subtypes and the housekeeping control human β -actin. White lines demarcate regions of gel images that were merged.

(B) Oxygen equilibrium curves (percentage oxyhemoglobin versus oxygen pressure [mm Hg]) for adult RBCs (●) and erythroblasts differentiated from X13 hiPSCs (day 27 post differentiation) from spinners 1 (■), 2 (▲), and 3 (▼) are shown.

(C) qRT-PCR quantified fold expression (*GAPDH*-normalized and relative to adult erythroblasts) of genes involved in erythroid maturation from X13 hiPSC-derived erythroblasts (day 27 post differentiation) terminally matured for 11 days (data represent the mean \pm SD of at least three independent replicates). Representative experiment shown.

(D) Change in cell diameter during differentiation in three independent spinner flask experiments. Day 28 erythroblasts were further matured until day 39.

(E) (Top) Giemsa staining and (bottom) flow cytometry evaluation for non-apoptotic (Annexin V⁻) enucleated RBCs (DRAQ5⁻) of X13 hiPSC erythroblasts after 21 days of terminal maturation without OP9 co-culture (No OP9), with monolayer OP9 co-culture (2D OP9), and with OP9-MC co-culture under agitation (3D OP9-MC). Red arrows indicate enucleated erythroid cells. Representative data from $n = 3$ independent experiments.

(F) Giemsa staining of terminally matured erythroblasts before and after processing through NWF filters is shown. Scale bar, 20 μ m. Bright-field images highlighting enucleated RBCs with biconcave appearance and SEM image of a single enucleated RBC are shown. Scale bar, 1 μ m. Arrows indicate the expelled pyrenocyte.

(G) Quantitative phase imaging data (mean \pm SD) for (i) cell volume, hiPSC RBCs were significantly greater compared with adult CD34 and adult blood; (ii) surface area, hiPSC RBCs were significantly higher compared with adult blood; (iii) sphericity, hiPSC RBCs were significantly greater compared with adult CD34 ($***p < 0.0001$) and adult blood ($*p < 0.05$); and (iv) refractive index tomography measurements for dynamic membrane fluctuations of RBCs, hiPSC RBCs were significantly lower compared with adult CD34 RBCs ($**p < 0.001$). RBCs were differentiated from adult CD34 cells ($n = 27$ cell counts) and hiPSCs ($n = 27$ cell counts) and adult blood ($n = 27$ cell counts).



switching from fetal to adult subtype (Trakarnsanga et al., 2014). Such strategies could be incorporated into genetically engineered hiPSCs to improve beta hemoglobin expression in the differentiated RBCs.

A major bottleneck for generation of hiPSC-RBCs is the rather low efficiency of enucleation of hiPSC-derived erythroblasts. Previously, transcriptomics and proteomics studies have raised the possibility of poor enucleation of hiPSC-derived erythroid cells due to defects in autophagy and lysosomal-mediated organelle clearance (Merryweather-Clarke et al., 2016) during terminal maturation and even possibly due to defects in cytoskeletal organization and remodeling (Trakarnsanga et al., 2019; Wilson et al., 2016). However, our transcriptomics analysis did not reveal any significant expression differences in some of these implicated genes (*VIM*, *TRIM58*, *VCPIP1*) between hiPSC- and adult-derived erythroid cells, at least at the erythroblast stage. Of genes whose expression differed significantly between adult and hiPSC erythroid cells, only two coincided with a list of 40 genes previously reported (Merryweather-Clarke et al., 2016; Trakarnsanga et al., 2019; Wilson et al., 2016). *ARID3A*, an erythroid transcription factor involved in cell cycle and transcriptional regulation was found to be significantly upregulated in hiPSC compared with adult erythroid cells. Second, *BCL11A*, a repressor of HbF, was found to be downregulated 3.5-fold in hiPSC compared with adult erythroid cells under conditions that favor erythroid expansion. This might explain the continued expression of HbF in hiPSC-derived erythroid cells. We found no differences in expression of genes involved in autophagy or cytoskeletal remodeling, as previously suggested (Merryweather-Clarke et al., 2016; Trakarnsanga et al., 2019; Wilson et al., 2016). These differences may partly be due to the different protocols used for differentiating hiPSC erythroid cells. Erythroid cells differentiated from our protocol had evidence of definitive erythropoiesis, such as adult beta hemoglobin expression, which was not demonstrated in the previous publications.

Here, we show that co-culture with stromal cells may help prevent erythroblast cell death and promote enucleation. Previous studies have reiterated this point with the use of OP9 and other stromal cell cultures (Giarratana et al., 2005; Lu et al., 2008; Suzuki et al., 1992). However, all these co-culture studies so far have been performed only in monolayer, making the scalability of this approach challenging. We show that a co-culture system using OP9 stromal cells can potentially be scaled up by culturing them on MCs, allowing the entire process to be performed in suspension culture and paving the way for future scale-up.

In conclusion, we have developed a suspension agitation culture differentiation process for differentiating hiPSCs toward erythroblasts that can be volumetrically scaled up. hiPSC-derived erythroid cells were capable of undergoing

enucleation, had expression of adult beta hemoglobin, albeit at reduced levels (in comparison with adult RBCs), were highly similar to adult-derived erythroid cells at the molecular level, and had similar membrane morphologies and dynamic membrane fluctuations/membrane deformability profiles. Further development would be necessary to adapt our differentiation processes into bioreactors for large-scale generation of high-density functional RBCs.

EXPERIMENTAL PROCEDURES

For details of this section, please also refer to the [Supplemental Experimental Procedures](#).

Briefly, all O-neg hiPSC lines were cultured on LN-521-coated MCs (Sivalingam et al., 2018) under static or agitation conditions for 7 days and subjected to hematopoietic mesoderm differentiation for 2 days using a combination of BMP4, Activin A, VEGF-165, B-FGF, and small-molecule CHIR-99021, as detailed in the [Supplemental Experimental Procedures](#). On day 3 of differentiation, single cells derived from MC aggregates following treatment with TrypLE Express and sieving of MCs were subjected to hematopoietic induction using a cocktail of cytokines (based on a protocol adapted from Olivier et al., 2016) for a further 8 days, under agitation. Then, the cells were further differentiated toward the erythroid lineage and expanded by fresh medium replenishment with cytokines and maintenance of cell seeding density at 5×10^5 to 1×10^6 cells/mL, under continuous agitation. Terminal maturation of erythroid cells was performed for a period of 2–3 weeks with or without co-culture of stromal cells, using IMDM supplemented with 10% human AB plasma, Holo-Transferrin, cytokines, and growth factors. The detailed protocol can be found in the [Supplemental Experimental Procedures](#).

Requests for materials should be addressed to the corresponding author.

Data and Code Availability

The authors declare that all data supporting the findings of this study are available within the article and its Supplemental Information files. Microarray data are available at Gene Expression Omnibus under accession no. GSE137917.

SUPPLEMENTAL INFORMATION

Supplemental Information can be found online at <https://doi.org/10.1016/j.stemcr.2020.11.008>.

AUTHOR CONTRIBUTIONS

S.K.W.O. was the principal investigator and takes primary responsibility for the article. J.S. performed all experiments, analyzed data, and wrote the manuscript. Y.S., H.Y.C., Z.R.L., H.K.T., and A.T.L.M. contributed toward the laboratory work. A.P.L., L.H.L., and A.H.M.T. performed the microarray study. T.W. performed bioinformatics. H.J.W., N.B.N., and B.M. performed the electron microscopy experiments. J.S., Y.S., B.M., L.R., S.R., Y.H.L., and



S.K.W.O. wrote the manuscript. Y.H.L. provided hiPSC lines for the study.

CONFLICTS OF INTERESTS

Dr. Steve Oh has patents on microcarrier technology for stem cell cultivation filed by A*STAR. He is also a founder of Zenzic Labs and SingCell. The rest of the authors declare no competing interests.

ACKNOWLEDGMENTS

This work was supported by a Joint Council Office grant from the Agency for Science, Technology and Research, Singapore (A*STAR) (1331AFG075), Singapore Immunology Network Core funding, A*STAR, and NUHS Start-Up funding (NUHSRO/2018/006/SU/01). The authors would like to thank Mickey Koh and team (Health Sciences Authority, Singapore) for useful discussions and Benedict and Dennis (EINST Technology Pte Ltd) for performing quantitative phase imaging using the Tomocube HT-2S system, Electron Microscopy Unit, National University of Singapore, and particularly Professor Ong Wei Yi, Miss Tan Suat Hoon, and Mister Lu Thong Beng. The authors would like to thank Naresh Waran Gnasegaran for providing a peripheral blood sample for this study.

Received: May 31, 2020

Revised: November 12, 2020

Accepted: November 12, 2020

Published: December 10, 2020

SUPPORTING CITATIONS

The following references appear in the supplemental information: Babicki et al., 2016; Chen et al., 2016; Clincke et al., 2013; Friebel and Meinke, 2006; Hong et al., 2010; Lee et al., 2017; Liu et al., 2013; Livak and Schmittgen, 2001; Lux, 2016; Malleret et al., 2013; Park et al., 2009; Sivalingam et al., 2016; Tan et al., 2014; Tao et al., 2011; Yu et al., 2007; Zhang et al., 2015.

REFERENCES

Allenby, M.C., Tahlawi, A., Morais, J.C.F., Li, K., Panoskaltis, N., and Mantalaris, A. (2018). Ceramic hollow fibre constructs for continuous perfusion and cell harvest from 3D hematopoietic organoids. *Stem Cells Int.* 2018, 6230214.

Alter, H.J., Stramer, S.L., and Dodd, R.Y. (2007). Emerging infectious diseases that threaten the blood supply. *Semin. Hematol.* 44, 32–41.

Angelos, M.G., Abrahante, J.E., Blum, R.H., and Kaufman, D.S. (2018). Single cell resolution of human hematoendothelial cells defines transcriptional signatures of hemogenic endothelium. *Stem Cells* 36, 206–217.

Babicki, S., Arndt, D., Marcu, A., Liang, Y., Grant, J.R., Maciejewski, A., and Wishart, D.S. (2016). Heatmapper: web-enabled heat mapping for all. *Nucleic Acids Res.* 44, W147–W153.

Bayley, R., Ahmed, F., Glen, K., McCall, M., Stacey, A., and Thomas, R. (2018). The productivity limit of manufacturing blood cell therapy in scalable stirred bioreactors. *J. Tissue Eng. Regen. Med.* 12, e368–e378.

Chen, H.Y., Tan, H.K., and Loh, Y.H. (2016). Derivation of transgene-free induced pluripotent stem cells from a single drop of blood. *Curr. Protoc. Stem Cell Biol.* 38, 4A 9 1–4A 9 10.

Christaki, E.E., Politou, M., Antonelou, M., Athanasopoulos, A., Simantirakis, E., Seghatchian, J., and Vassilopoulos, G. (2019). Ex vivo generation of transfusable red blood cells from various stem cell sources: a concise revisit of where we are now. *Transfus. Apher. Sci.* 58, 108–112.

Clincke, M.F., Molleryd, C., Zhang, Y., Lindskog, E., Walsh, K., and Chotteau, V. (2013). Very high density of CHO cells in perfusion by ATF or TFF in WAVE bioreactor. Part I. Effect of the cell density on the process. *Biotechnol. Prog.* 29, 754–767.

Dorn, I., Klich, K., Arauzo-Bravo, M.J., Radstaak, M., Santourlidis, S., Ghanjati, F., Radke, T.F., Psathaki, O.E., Hargus, G., Kramer, J., et al. (2015). Erythroid differentiation of human induced pluripotent stem cells is independent of donor cell type of origin. *Haematologica* 100, 32–41.

Friebel, M., and Meinke, M. (2006). Model function to calculate the refractive index of native hemoglobin in the wavelength range of 250–1100 nm dependent on concentration. *Appl. Opt.* 45, 2838–2842.

Giarratana, M.C., Kobari, L., Lapillonne, H., Chalmers, D., Kiger, L., Cynober, T., Marden, M.C., Wajcman, H., and Douay, L. (2005). Ex vivo generation of fully mature human red blood cells from hematopoietic stem cells. *Nat. Biotechnol.* 23, 69–74.

Hassell, T., Gleave, S., and Butler, M. (1991). Growth inhibition in animal cell culture. The effect of lactate and ammonia. *Appl. Biochem. Biotechnol.* 30, 29–41.

Hirani, R., Wong, J., Diaz, P., Mondy, P., Hogan, C., Dennington, P.M., Pink, J., and Irving, D.O. (2017). A national review of the clinical use of group O D- red blood cell units. *Transfusion* 57, 1254–1261.

Hirose, S., Takayama, N., Nakamura, S., Nagasawa, K., Ochi, K., Hirata, S., Yamazaki, S., Yamaguchi, T., Otsu, M., and Sano, S. (2013). Immortalization of erythroblasts by c-MYC and BCL-XL enables large-scale erythrocyte production from human pluripotent stem cells. *Stem Cell Reports* 1, 499–508.

Hong, S.H., Werbowetski-Ogilvie, T., Ramos-Mejia, V., Lee, J.B., and Bhatia, M. (2010). Multiparameter comparisons of embryoid body differentiation toward human stem cell applications. *Stem Cell Res.* 5, 120–130.

Kim, G., Lee, M., Youn, S., Lee, E., Kwon, D., Shin, J., Lee, S., Lee, Y.S., and Park, Y. (2018). Measurements of three-dimensional refractive index tomography and membrane deformability of live erythrocytes from *Pelophylax nigromaculatus*. *Sci. Rep.* 8, 9192.

Kurita, R., Suda, N., Sudo, K., Miharada, K., Hiroshima, T., Miyoshi, H., Tani, K., and Nakamura, Y. (2013). Establishment of immortalized human erythroid progenitor cell lines able to produce enucleated red blood cells. *PLoS One* 8, e59890.

Lam, A.T., Chen, A.K., Ting, S.Q., Reuveny, S., and Oh, S.K. (2016). Integrated processes for expansion and differentiation of human pluripotent stem cells in suspended microcarrier cultures. *Biochem. Biophys. Res. Commun.* 473, 764–768.

Lee, S., Park, H., Kim, K., Sohn, Y., Jang, S., and Park, Y. (2017). Refractive index tomograms and dynamic membrane fluctuations



- of red blood cells from patients with diabetes mellitus. *Sci. Rep.* 7, 1039.
- Leonard, M., Brice, M., Engel, J.D., and Papayannopoulou, T. (1993). Dynamics of GATA transcription factor expression during erythroid differentiation. *Blood* 82, 1071–1079.
- Liu, F., Bhang, S.H., Arentson, E., Sawada, A., Kim, C.K., Kang, I., Yu, J., Sakurai, N., Kim, S.H., Yoo, J.J., et al. (2013). Enhanced hemangioblast generation and improved vascular repair and regeneration from embryonic stem cells by defined transcription factors. *Stem Cell Reports* 1, 166–182.
- Livak, K.J., and Schmittgen, T.D. (2001). Analysis of relative gene expression data using real-time quantitative PCR and the 2⁻(Delta Delta C(T)) Method. *Methods* 25, 402–408.
- Lu, S.J., Feng, Q., Park, J.S., Vida, L., Lee, B.S., Strausbauch, M., Wettstein, P.J., Honig, G.R., and Lanza, R. (2008). Biologic properties and enucleation of red blood cells from human embryonic stem cells. *Blood* 112, 4475–4484.
- Lux, S.E.t. (2016). Anatomy of the red cell membrane skeleton: unanswered questions. *Blood* 127, 187–199.
- Malleret, B., Xu, F., Mohandas, N., Suwanarusk, R., Chu, C., Leite, J.A., Low, K., Turner, C., Sriprawat, K., Zhang, R., et al. (2013). Significant biochemical, biophysical and metabolic diversity in circulating human cord blood reticulocytes. *PLoS One* 8, e76062.
- Mao, B., Huang, S., Lu, X., Sun, W., Zhou, Y., Pan, X., Yu, J., Lai, M., Chen, B., Zhou, Q., et al. (2016). Early development of definitive erythroblasts from human pluripotent stem cells defined by expression of glycophorin A/CD235a, CD34, and CD36. *Stem Cell Reports* 7, 869–883.
- Merryweather-Clarke, A.T., Tipping, A.J., Lamikanra, A.A., Fa, R., Abu-Jamous, B., Tsang, H.P., Carpenter, L., Robson, K.J., Nandi, A.K., and Roberts, D.J. (2016). Distinct gene expression program dynamics during erythropoiesis from human induced pluripotent stem cells compared with adult and cord blood progenitors. *BMC Genomics* 17, 817.
- Olivier, E.N., Marenah, L., McCahill, A., Condie, A., Cowan, S., and Mountford, J.C. (2016). High-efficiency serum-free feeder-free erythroid differentiation of human pluripotent stem cells using small molecules. *Stem Cells Transl. Med.* 5, 1394–1405.
- Paes, B., Moco, P.D., Pereira, C.G., Porto, G.S., de Sousa Russo, E.M., Reis, L.C.J., Covas, D.T., and Picanco-Castro, V. (2017). Ten years of iPSC: clinical potential and advances in vitro hematopoietic differentiation. *Cell Biol. Toxicol.* 33, 233–250.
- Park, Y., Yamauchi, T., Choi, W., Dasari, R., and Feld, M.S. (2009). Spectroscopic phase microscopy for quantifying hemoglobin concentrations in intact red blood cells. *Opt. Lett.* 34, 3668–3670.
- Peyrard, T., Bardiaux, L., Krause, C., Kobari, L., Lapillonne, H., Andreu, G., and Douay, L. (2011). Banking of pluripotent adult stem cells as an unlimited source for red blood cell production: potential applications for alloimmunized patients and rare blood challenges. *Transfus. Med. Rev.* 25, 206–216.
- Sivalingam, J., Chen, H.Y., Yang, B.X., Lim, Z.R., Lam, A.T.L., Woo, T.L., Chen, A.K., Reuveny, S., Loh, Y.H., and Oh, S.K. (2018). Improved erythroid differentiation of multiple human pluripotent stem cell lines in microcarrier culture by modulation of Wnt/beta-Catenin signaling. *Haematologica* 103, e279–e283.
- Sivalingam, J., Lam, A.T., Chen, H.Y., Yang, B.X., Chen, A.K., Reuveny, S., Loh, Y.H., and Oh, S.K. (2016). Superior red blood cell generation from human pluripotent stem cells through a novel microcarrier-based embryoid body platform. *Tissue Eng. C Methods* 22, 765–780.
- Sturgeon, C.M., Ditadi, A., Awong, G., Kennedy, M., and Keller, G. (2014). Wnt signaling controls the specification of definitive and primitive hematopoiesis from human pluripotent stem cells. *Nat. Biotechnol.* 32, 554–561.
- Suzuki, J., Fujita, J., Taniguchi, S., Sugimoto, K., and Mori, K.J. (1992). Characterization of murine hemopoietic-supportive (MS-1 and MS-5) and non-supportive (MS-K) cell lines. *Leukemia* 6, 452–458.
- Tan, H.K., Toh, C.X., Ma, D., Yang, B., Liu, T.M., Lu, J., Wong, C.W., Tan, T.K., Li, H., Syn, C., et al. (2014). Human finger-prick induced pluripotent stem cells facilitate the development of stem cell banking. *Stem Cells Transl. Med.* 3, 586–598.
- Tao, Z.Y., Xia, H., Cao, J., and Gao, Q. (2011). Development and evaluation of a prototype non-woven fabric filter for purification of malaria-infected blood. *Malar. J.* 10, 251.
- Trakarnsanga, K., Ferguson, D., Daniels, D.E., Griffiths, R.E., Wilson, M.C., Mordue, K.E., Gartner, A., Andrienko, T.N., Calvert, A., Condie, A., et al. (2019). Vimentin expression is retained in erythroid cells differentiated from human iPSC and ESC and indicates dysregulation in these cells early in differentiation. *Stem Cell Res. Ther.* 10, 130.
- Trakarnsanga, K., Wilson, M.C., Lau, W., Singleton, B.K., Parsons, S.F., Sakuntanaga, P., Kurita, R., Nakamura, Y., Anstee, D.J., and Frayne, J. (2014). Induction of adult levels of beta-globin in human erythroid cells that intrinsically express embryonic or fetal globin by transduction with KLF1 and BCL11A-XL. *Haematologica* 99, 1677–1685.
- Trakarnsanga, K., Griffiths, R.E., Wilson, M.C., Blair, A., Satchwell, T.J., and Meinders, M. (2017). An immortalized adult human erythroid line facilitates sustainable and scalable generation of functional red cells. *Nat. Commun.* 8, 14750.
- Wilson, M.C., Trakarnsanga, K., Heesom, K.J., Cogan, N., Green, C., Toyne, A.M., Parsons, S.F., Anstee, D.J., and Frayne, J. (2016). Comparison of the proteome of adult and cord erythroid cells, and changes in the proteome following reticulocyte maturation. *Mol. Cell Proteomics* 15, 1938–1946.
- Ying Wang, Y.G., He, C., Ye, Z., Gerecht, S., and Cheng, L. (2016). Scalable production of human erythrocytes from induced pluripotent stem cells. *BioRxiv* <https://doi.org/10.1101/050021>.
- Yu, J., Vodyanik, M.A., Smuga-Otto, K., Antosiewicz-Bourget, J., Frane, J.L., Tian, S., Nie, J., Jonsdottir, G.A., Ruotti, V., Stewart, R., et al. (2007). Induced pluripotent stem cell lines derived from human somatic cells. *Science* 318, 1917–1920.
- Zhang, Y., Stobbe, P., Silvander, C.O., and Chotteau, V. (2015). Very high cell density perfusion of CHO cells anchored in a non-woven matrix-based bioreactor. *J. Biotechnol.* 213, 28–41.
- Zhang, Y., Wang, C., Wang, L., Shen, B., Guan, X., Tian, J., Ren, Z., Ding, X., Ma, Y., Dai, W., et al. (2017). Large-scale ex vivo generation of human red blood cells from cord blood CD34(+) cells. *Stem Cells Transl. Med.* 6, 1698–1709.

Stem Cell Reports, Volume 16

Supplemental Information

**A Scalable Suspension Platform for Generating High-Density Cultures
of Universal Red Blood Cells from Human Induced Pluripotent Stem
Cells**

**Jaichandran Sivalingam, Yu SuE, Zhong Ri Lim, Alan T.L. Lam, Alison P. Lee, Hsueh Lee
Lim, Hong Yu Chen, Hong Kee Tan, Tushar Warriar, Jing Wen Hang, Nazmi B. Nazir, Andy
H.M. Tan, Laurent Renia, Yui Han Loh, Shaul Reuveny, Benoit Malleret, and Steve K.W.
Oh**

Supplementary Information

A scalable suspension platform for generation of high density cultures of universal red blood cells from human induced pluripotent stem cells

Jaichandran Sivalingam, Yu SuE, Lim Zhong Ri, Alan Tin Lun Lam, Alison P.Lee, Hsueh Lee Lim, Hong Yu Chen, Hong Kee Tan, Tushar Warriar, Jing Wen Hang, Nazmi B.Nazir, Andy Hee Meng Tan, Laurent Renia, Yui Han Loh, Shaul Reuveny, Benoit Malleret and Steve Kah Weng Oh.

Inventory of Supplemental Information

Supplemental Table and Figures

Table S1: List of genes identified based on publication for comparison of erythroid cells differentiated from hiPSC and adult CD34 cells.

Table S2. List of primers used in this study.

Figure S1: Overview of agitation suspension culture differentiation platform.

Figure S2: Characterization of hiPSC erythroid cells differentiated in shake-flasks.

Figure S3: Characterization of hiPSC erythroid cells differentiated in shake-flasks.

Figure S4: Spinner culture differentiation of fibroblast derived hiPSC FR202.

Figure S5: Transcriptome analysis of HiPSC vs Adult differentiated erythroid cells.

Figure S6: Terminal maturation and functional characterization of hiPSC and adult CD34 differentiated RBCs.

Figure S7: Terminal maturation and functional characterization of hiPSC and adult CD34 differentiated RBCs.

Supplemental Experimental Procedures

Figure S1 Development of agitation suspension culture differentiation protocol

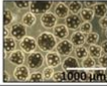
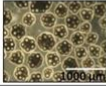
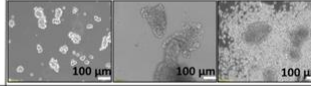






		Stage	iPSC expansion	Mesoderm induction	Hematopoietic induction	Erythroblast expansion	Erythroblast maturation
		Duration	7 days	3 days	14 days	14 days	14-21 days
		Medium	mTeSR1	Stemline II Day 0: BMP4, VEGF, Activin A, CHIR Day 1: BMP4, VEGF, Activin A Day 2: BMP4, VEGF, Activin A, bFGF, β -Estradiol, SCF	Stemline II Day 3: BMP4, VEGF, bFGF, β -Estradiol, SCF, IGF2, TPO, Heparin, IBMX Day 7: BMP4, VEGF, bFGF, β -Estradiol, SCF, IGF2, TPO, Heparin, IBMX, SR1 Day 11: BMP4, SCF, Flt3-L, IL3, EPO, IBMX	Stemline II SCF, EPO, IL3, hydrocortisone, holo-transferrin, Erycte, Serum Replacement 3, Pluripotin	IMDM EPO, 10% human plasma, holo-transferrin, insulin, mifipristone
		Culture condition	Agitation	Agitation	Agitation	Agitation	Agitation
							
Scalable culture platform							
6 well ULA plates		Seeding density: Fold-expansion: Total volume: Expanded cell numbers:	2 x 10 ⁵ cells/ml 10-14 5 ml 1-1.4 x 10 ⁷	1 x 10 ⁶ cells/ml 1-3 5 ml 2.5-7.5 x 10 ⁷	1.25 -1.75 x 10 ⁵ cells/ml 10-30 5 ml 0.625 - 2.67 x 10 ⁷	2.5 x 10 ⁵ cells/ml 100 5 ml 1.25 x 10 ⁸	1 x 10 ⁶ cells/ml N.A 5 ml 5 x 10 ⁶
		Seeding density : Fold-expansion : Total volume: Expanded cell numbers:	2 x 10 ⁵ cells/ml 10-14 5 ml 1-1.4 x 10 ⁷	1 x 10 ⁶ cells/ml 1-3 5 ml 5 x 10 ⁶	Seeding density: 1.25 -1.75 x 10 ⁵ cells/ml Fold-expansion: 10-30 Total volume: 10 ml Expanded cell numbers: 1.25 - 5.25 x 10 ⁷	2.5 x 10 ⁵ cells/ml 100 10 ml 2.5 x 10 ⁸	1 x 10 ⁶ cells/ml N.A 10 ml 1 x 10 ⁷
125 ml spinner flasks		Seeding density: Fold-expansion: Total volume: Expanded cell numbers:	2 x 10 ⁵ cells/ml 10 50 ml 1.25 x 10 ⁸	1.2 x 10 ⁶ cells/ml 1-1.4 50 ml 8.2 x 10 ⁷	2.5 x 10 ⁵ cells/ml 10-30 50 ml 1.25 - 3.75 x 10 ⁸	2.5 x 10 ⁵ cells/ml 100 100 ml 1 x 10 ⁹	1 x 10 ⁶ cells/ml N.A 100 ml 1 x 10 ⁸
							

Figure S1: Overview of agitation suspension culture differentiation platform. Schematic of suspension culture continuous agitation differentiation process comprising of hiPSC expansion, mesoderm induction, hematopoietic induction, erythroblast expansion and erythroblast maturation. Representative bright-field images of microcarrier-cell aggregates and/or differentiating cells are shown. The differentiation process was progressively scaled-up from 6 well ULA plates to 50 shaker flasks to 125 ml spinner flasks. The initial seeding density, fold-expansion, total volume and total cells derived after expansion are reported for each stage of differentiation.

Figure S2 Hematopoietic differentiation from hemogenic endothelial clusters in suspension differentiation protocol

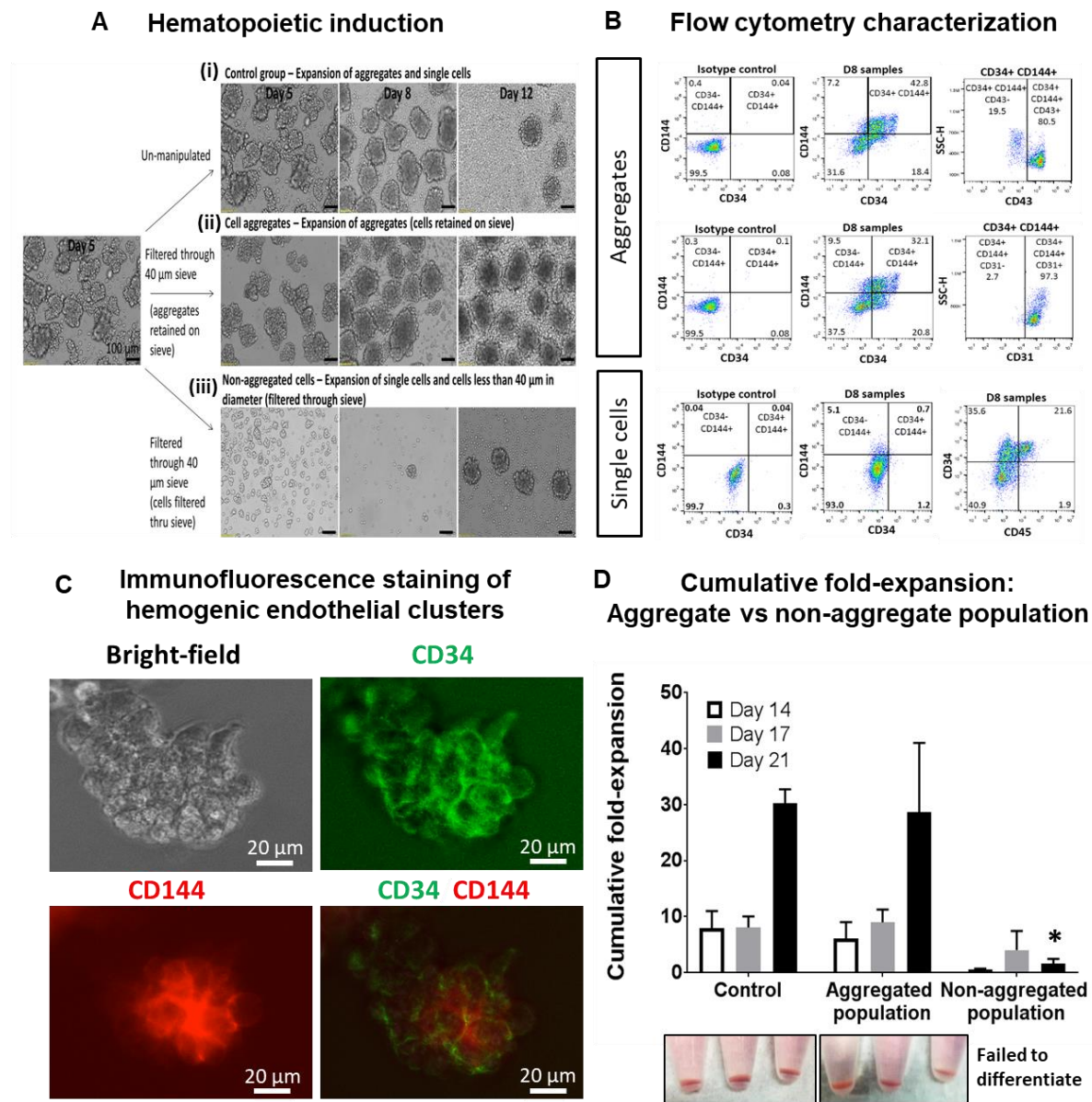
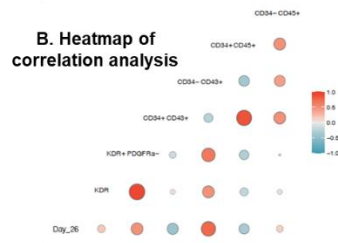
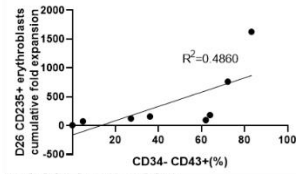


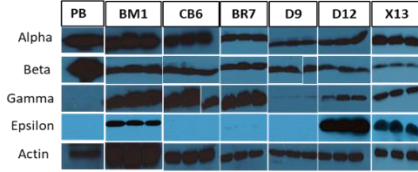
Figure S2: Characterization of hiPSC erythroid cells differentiated in shake-flasks. (A) At day 5 of differentiation, small aggregates and single cells are observed. Differentiation was performed on 3 experimental groups as follows: (i) Un-manipulated control group consisting of aggregates and single cells; (ii) cell aggregates retained following straining through 40 μ m cell-strainers; (iii) single cells derived following straining through 40 μ m cell-strainers. Representative bright-field images of differentiating cells from day 5 - day 12 are shown. (B) Cells from un-manipulated control group on day 8 of differentiation were separated by straining into aggregate and single cell population and characterized by FACS for identification of hemogenic endothelial population (CD34+CD144+CD31+/CD43+) and pan-hematopoietic progenitors (CD34+CD45+). (C) Immunofluorescence staining of day 8 cell aggregates identifies hemogenic endothelial clusters with co-expression of CD34 (green) and CD144 (red) markers. (D) Cumulative fold-expansion of differentiated cells following 21 days of differentiation of cells from groups I (control), II (aggregated population) and III (non-aggregated population). Data represent mean \pm SD with at least 3 independent replicates. Corresponding hemoglobinized cell pellets are shown below graph. Note that single cells from non-aggregated population failed to differentiate further.

Figure S3 Characterization of hiPSC erythroid cells differentiated in shake-flasks

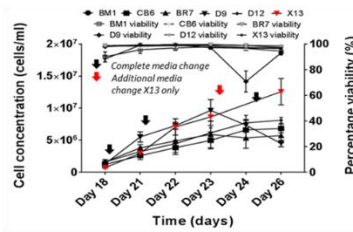
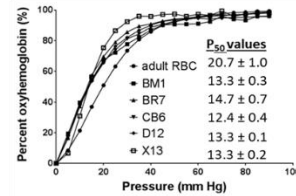
A. Correlation analysis between the D26 erythroblasts yield and CD34- CD43+ marker of 8 hiPSC cell lines



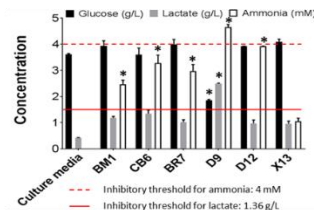
C. Hemoglobin Immunoblot



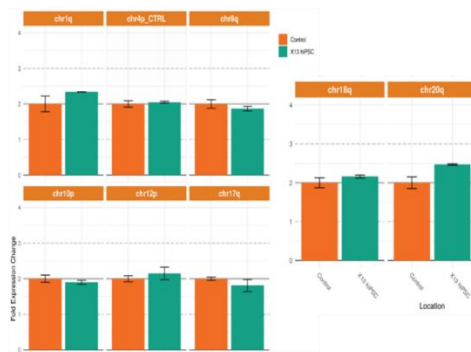
D. Oxygen equilibration



F. Metabolite measurements



G. Pluripotent stem cell Genetic Analysis



H. iCS-digital™ Pluri test



Figure S3: Characterization of hiPSC erythroid cells differentiated in shake-flasks. (A) Correlation analysis between the D26 erythroblasts yield and CD34- CD43+ marker of 8 hiPSC cell lines. (B) Heatmap of correlation analysis between the D26 erythroblasts yield and different hematopoietic markers. (C) Cell lysates from peripheral blood (PB) and erythroblasts differentiated from BM1, CB6, BR7, D9 and D12 (day 26 post differentiation) were immunoblotted with alpha, beta, gamma, epsilon human hemoglobin subtypes. *Insufficient samples for IMR90 and FR202. (D) Oxygen equilibrium curves of adult RBCs (●), hiPSC differentiated erythroblasts BM1 (■), BR7 (▲), CB6 (▼), D12 (◆) and X13 (□). Corresponding p₅₀ values are presented. *Insufficient samples for IMR90, FR202 and D9. (E) Cell concentration (cells/ml) and % viability during erythroblast expansion. Black arrows indicate complete media change for all cultures while red arrow indicates additional complete media change for X13 only. (F) Measurements of glucose (g/L), lactate (g/L) and ammonia (mM) from culture supernatants of different hiPSC erythroid cells and fresh culture media on day 24 of differentiation. Red solid and dotted lines indicate inhibitory threshold for lactate (1.36 g/L) and ammonia (4 mM) respectively. *p<0.05 for comparison against X13. (G) Recurrent karyotypic abnormalities in hiPSCs were evaluated by a qPCR-based method using hiPSC genetic analysis kit. Graphical representation of copy numbers for each locus for normal control genomic DNA and X13 hiPSC line are shown. (H) Genomic DNA extracted from X13 hiPSC derived erythroblasts (Day 24 of differentiation) were subjected to iCS-digital™ pluri test to evaluate for common genomic abnormalities. (Top) Copy number values of 24 genomic regions evaluated and colour coded accordingly (Loss (orange): 1 to 1.4 copies; Normal (green): 1.6 to 2.4; Gain (purple): 2.6 to 3) show normal copies for X13 erythroblast. (Bottom): Graphical representation of copy number values for each of the 24 chromosomal regions evaluated for X13 erythroblasts. Statistical tests were performed on the pooled data from at least 3 independent replicates.

Figure S4 Scale-up of hiPSC differentiation in 125 ml and 500 ml spinner flasks

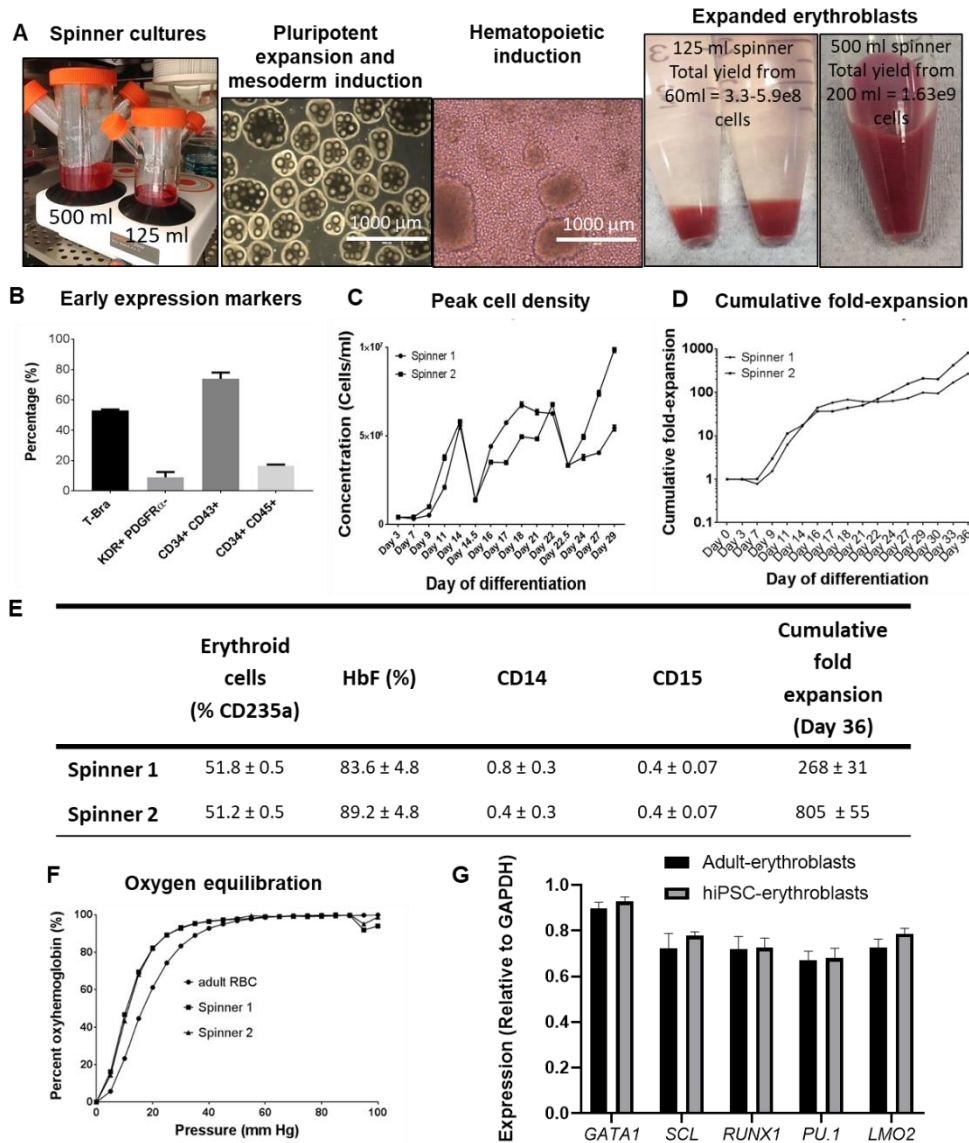


Figure S4: Spinner culture differentiation of fibroblast derived hiPSC FR202. (A) Image showing hiPSC erythroid cells cultured in 125ml and 500ml spinner culture flasks, MC-hiPSC cell aggregates during pluripotent expansion and mesoderm of differentiation, single cells and aggregates during hematopoietic induction and hemoglobinized erythroblast cell pellets from 125ml and 500ml spinner flasks (total number of cells indicated in image) respectively at the end of culture period (Day 30-36). (B) FACS percentage of cells expressing primitive streak/early mesoderm marker (T-bra), hematopoietic mesoderm marker (KDR+PDGFR α -) and hematopoietic progenitor markers (CD34+CD43+ and CD34+CD45+). (C) Cell concentration and (D) cumulative fold-expansion during the differentiation process in spinner culture flasks. Arrows indicate time-points when cells were reseeded at low density. (E) Table showing FACS summary of CD235a+ erythroid cells, fetal hemoglobin (HbF), myelomonocytic populations (CD14/CD15) and cumulative fold expansion on day 36 of differentiation. (F) Oxygen equilibrium curves of adult RBCs (●) and FR202 differentiated erythroblasts (Day 36 post differentiation) from spinner flasks 1 (■) and 2 (▲). Corresponding p50 values are presented. (G) Comparison between erythroid cells differentiated from adult CD34+ and from hiPSCs based on microarray data. There is no significant difference in the erythropoiesis induction related gene expression levels (in Fig. 3F) between the adult and hiPSC derived erythroblasts. The graph above represents these values after normalization to a control gene (*GAPDH*). Statistical tests were performed on the pooled data from at least 3 independent replicates.

Figure S5 Transcriptome analysis of HiPSC vs Adult differentiated erythroid cells

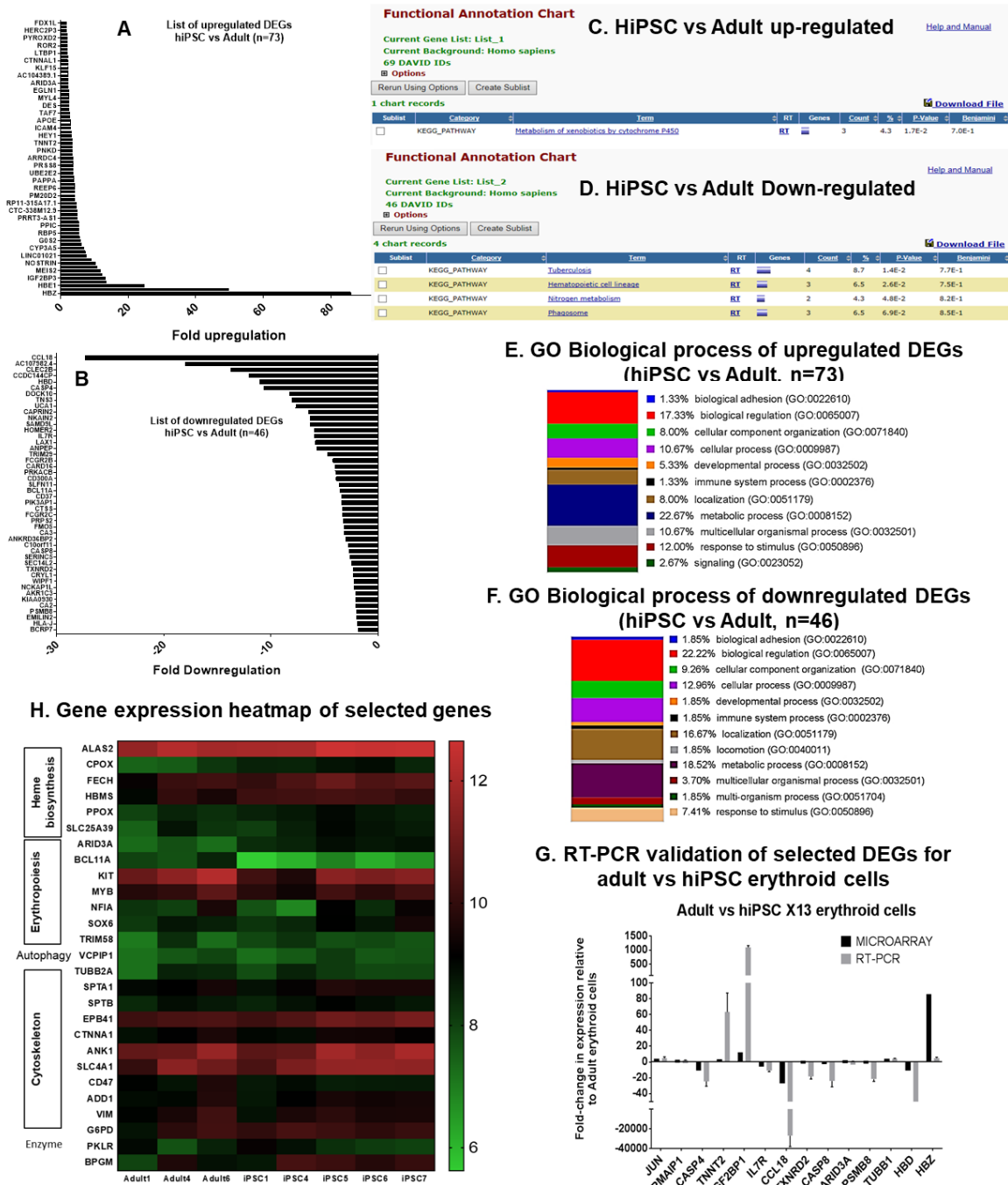


Figure S5: Transcriptome analysis of HiPSC vs Adult differentiated erythroid cells. Fold-change in expression of (A) up-regulated and (B) down-regulated DEG for comparison of erythroid cells from hiPSC vs Adult (X13 donor). Mapping of hiPSC vs adult (C) upregulated DEGs and (D) downregulated DEGs using DAVID Functional annotation analysis. Bar chart showing gene ontology of biological processes of (E) upregulated and (F) downregulated DEGs for comparison of erythroid cells from hiPSC vs Adult. (G) Comparison of fold-change in DEGs of hiPSC differentiated erythroid cells relative to adult differentiated erythroid cells validated by RT-PCR in comparison with microarray outcomes. (H) Heatmap (normalized expression signal intensity) of selected genes based on publications categorized according to molecular functions (heme biosynthesis, erythropoiesis, autophagy, cytoskeleton, enzyme) for comparison between adult and hiPSC samples.

Figure S6 Terminal maturation and functional characterization of hiPSC erythroblast

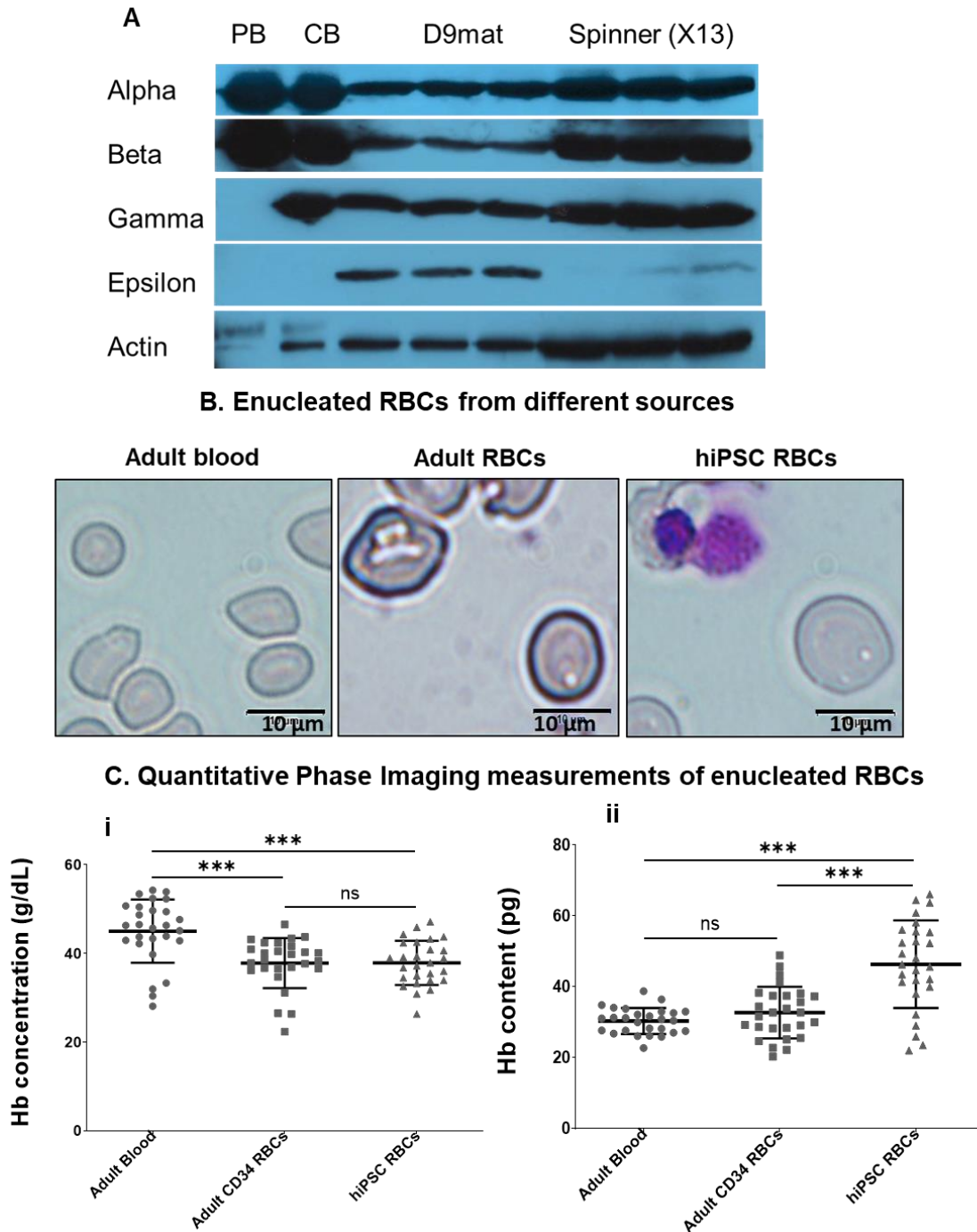
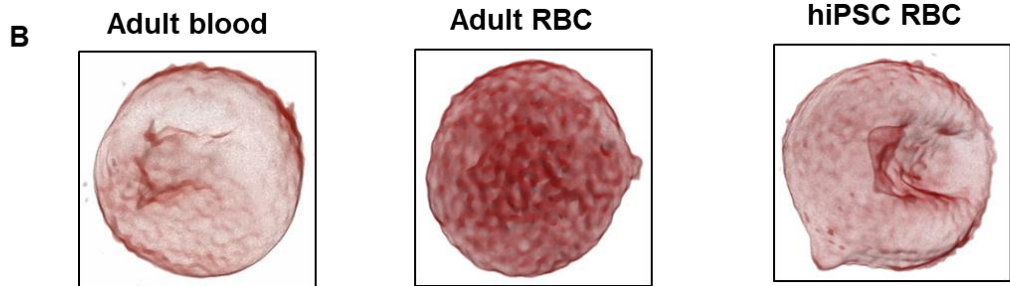
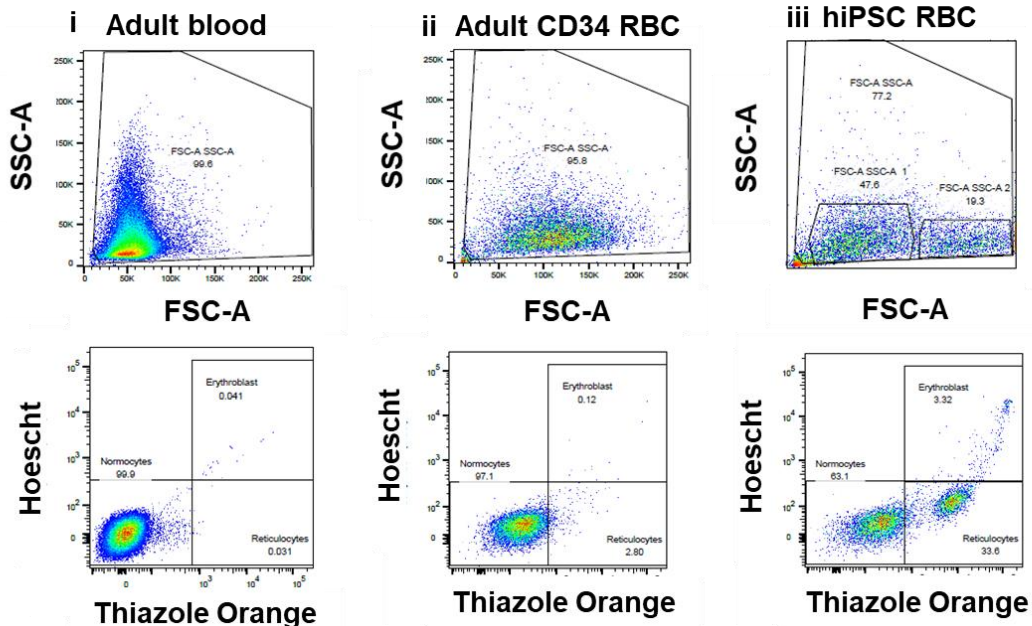


Figure S6: Terminal maturation and functional characterization of hiPSC and adult CD34 differentiated RBCs. (A) Entire western blot with expression of globin subtypes that shown in Figure 5A (CB and D9 mat are not involved in this study). (B) Giemsa staining of enucleated RBCs from adult blood, Adult differentiated RBCs and hiPSC differentiated RBCs. Scale=10 micron. (C) Quantitative phase imaging data for (i) Hb concentration and (ii) Hb content measurements for RBCs from the 3 different populations using a HT-2S Holotomographic microscope.

Figure S7 Terminal maturation and functional characterization of hiPSC erythroblast

A. Flow cytometry characterization of reticulocyte and normocyte populations



C. Electron microscopy imaging of enucleated RBCs

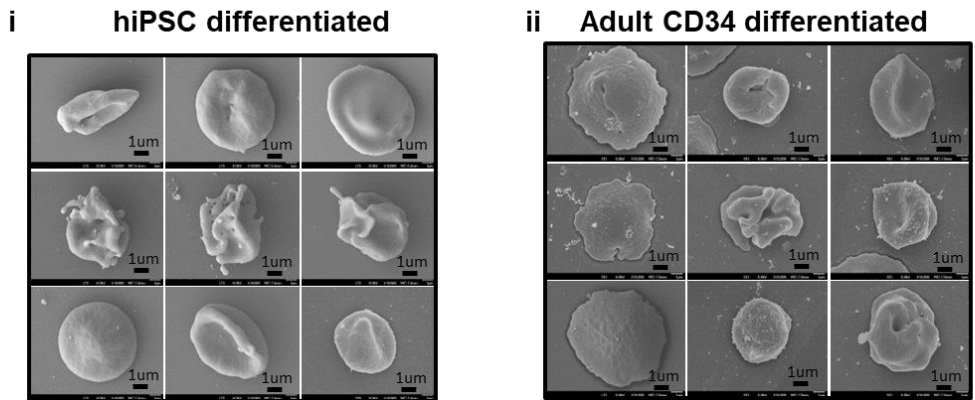


Figure S7: Terminal maturation and functional characterization of hiPSC and adult CD34 differentiated RBCs. (A) Flow cytometry characterization of purified RBCs from (i) adult blood and in vitro differentiation of (ii) adult CD34 and (iii) hiPSCs. Cells were stained with Hoechst and Thiazole Orange dyes to quantify percentage of normocytes, reticulocytes and erythroblast which are identified in their specific quadrants in the flow cytometry plots. (B) 3D-tomography representative images and (C) scanning electron microscopy images of enucleated RBCs from the respective groups. Scale=1 micron.

Supplemental Experimental Procedures

Monolayer pluripotent cell culture

O-neg hiPSC lines (D5, D9, D12, X13, BR7) were reprogrammed from CD71+ erythroblasts, derived from finger-prick blood of consented human donors (with approval from the ethics committee of the National University of Singapore; approval number NUS 1957) as detailed previously (Chen et al., 2016, Tan et al., 2014). FR202 was reprogrammed similarly using dermal fibroblasts. IMR90-iPSC was kindly provided by James Thompson's lab (Yu et al., 2007). BM1 (IISH1i-BM1) and CB6 (IISH3i-CB6) hiPSCs were purchased from WiCell Research Institute. All hiPSC lines were cultured as detailed previously (Sivalingam et al., 2016).

Microcarrier pluripotent cell culture

Culture of hiPSCs on MCs has previously been described (Sivalingam et al., 2018, Sivalingam et al., 2016). 3D MC-hiPSCs were cultured under continuous agitation in an agitated platform at 75 rpm for 7 days with daily medium changes. For initiation of spinner cultures, hiPSC-MCs initially cultured for 7 days under static condition in 6 well ULA plates were manually broken into small aggregates by gentle pipetting and seeded in 50 ml of mTeSRTM1 medium at a density of 2×10^5 cells/ml. Cells were cultured in 125 ml spinner flasks (Corning) at 36 rpm with 90% medium change daily for 7 days.

Hematopoietic mesoderm induction of hiPSC-MC aggregates

HPSC-MC aggregates (1×10^6 cells/ml) were transferred to mesoderm induction medium composed of cytokines plus Stemline ®II Hematopoietic Stem Cell Expansion medium (SL2) (Sigma-Aldrich) in either 6 well ULA plates (5 ml) under continuous agitation at 75 rpm or 125 ml spinner flasks (50 ml) under continuous agitation at 36 rpm. Daily medium changes as indicated: **Day 0**- SL2 supplemented with 30 ng/ml BMP4 (R&D systems), 50 ng/ml VEGF-165 (Peprotech), 40 ng/ml Activin A (StemcellTM Technologies), 15 μ M CHIR-99021 (Selleckchem); **Day 1**- SL2 supplemented with 30 ng/ml BMP4, 50 ng/ml VEGF-165, 40 ng/ml Activin A; **Day 2** - SL2 supplemented with 20 ng/ml BMP4, 30 ng/ml VEGF-165, 5 ng/ml Activin A, 10 ng/ml bFGF (Peprotech), 20 ng/ml SCF (R&D systems) and 0.4 ng/ml β -estradiol (Sigma-Aldrich). Samples were collected on day 1 and day 3 for flow cytometry analysis of T-brachyury (T-Bra) and KDR+ cells, respectively.

Hematopoietic induction of cells derived from hiPSC-MC aggregates

On day 3 of differentiation, single cells were derived from hiPSC-MC aggregates following treatment with TrypLETM Express (ThermoFisher Scientific) at 37°C for 5 min followed by straining through 40 μ m cell strainers (Greiner Bio-one, Germany). Cells were seeded at $1 - 2 \times 10^5$ cells/ml in hematopoietic induction medium (adapted from Olivier *et al* (Olivier et al., 2016)) in either 6 well ULA plates (5 ml), 50 ml shake-flasks (10 ml), 125 ml spinner flasks (50 ml) or 500 ml spinner flasks (100 ml). Complete medium changes (unless otherwise stated) as indicated: **Day 3**- SL2 supplemented with 20 ng/ml BMP4, 30 ng/ml VEGF-165, 10 ng/ml bFGF, 30 ng/ml SCF, 10 ng/ml IGF2 (StemcellTM Technologies), 10 ng/ml TPO (Peprotech), 5 U/ml Heparin (Sigma-Aldrich), 50 μ M 3-Isobutyl-1-methylxanthine (IBMX)(Sigma-Aldrich), 0.4 ng/ml β -estradiol; **Day 5**- Top-up 1:6 with SL2 supplemented with 120 ng/ml BMP4, 180 ng/ml VEGF-165, 60 ng/ml bFGF, 180 ng/ml SCF, 60 ng/ml IGF2, 60 ng/ml TPO, 30 U Heparin, 300 μ M IBMX and 2.4 ng/ml β -estradiol; **Day 7** – SL2 supplemented with 20 ng/ml BMP4, 30 ng/ml VEGF, 10 ng/ml bFGF, 30 ng/ml SCF, 10 ng/ml IGF2, 10 ng/ml TPO, 5 U Heparin, 50 μ M IBMX, 0.4 ng/ml β -estradiol. **Day 9** - Top-up 1:2 with SL2 supplemented with 20 ng/ml BMP4, 30 ng/ml VEGF-165, 10 ng/ml bFGF, 30 ng/ml SCF, 10 ng/ml IGF2, 10 ng/ml TPO, 5 U Heparin, 50 μ M IBMX and 0.4 ng/ml β -estradiol.

Erythroid induction of cells derived from hiPSC-MC aggregates

Cells were seeded at $1 - 2.5 \times 10^5$ cells/ml in erythroid induction medium in either 6 well ULA plates (5 ml), 50 ml shake-flasks (10 ml) or 125 ml and 500 ml spinner flasks (50 -100 ml). Complete medium changes (unless otherwise stated) as indicated: **Day 11**- SL2 supplemented with 6.7 ng/ml BMP4, 30 ng/ml SCF, 50 μ M IBMX, 1 μ M hydrocortisone (Sigma-Aldrich), 16.7 ng/ml Flt3L (Peprotech), 6.7 ng/ml IL3 (Peprotech), 4 U/ml EPO (Peprotech); **Day 13**- Top-up 1:6 with SL2 supplemented with 40.2 ng/ml BMP4, 180 ng/ml SCF, 300 μ M IBMX, 6 μ M hydrocortisone (Sigma-Aldrich), 100.2 ng/ml Flt3L, 40.2 ng/ml IL3, 24 U/ml EPO, 3 μ M Pluripotin (Sigma-Aldrich); **Day 15 onwards** - SL2 supplemented with 1X serum replacement 3 (Sigma-Aldrich), 0.3% v/v ExCyte reagent (Millipore), 1 μ M hydrocortisone, 100 ng/ml SCF, 4 U/ml EPO, 10 ng/ml IL3, 0.2 mg/ml holotransferrin (MP Biomedicals) and 1X Penicillin and Streptomycin (Gibco). Cumulative fold-expansion was calculated by multiplying fold-expansion achieved between passaging of cells over the course of study.

Terminal maturation of erythroid cells

Terminal maturation of erythroid cells was induced by transferring cells to maturation medium ($1-2 \times 10^6$ cells/ml) for 14-21 days with medium change every 3 days; Iscove's Modified Dulbecco's medium (IMDM) (ThermoFisher Scientific) supplemented with 10% human plasma (Innovative™ Research), 10 ng/ml human recombinant insulin (Gibco), 6 U/ml EPO, 1 μ M mifepristone, 500 μ g/ml holo-transferrin and 1X Penicillin-Streptomycin. In some experiments, erythroid cells were co-cultured with bone-marrow derived primary human MSCs or murine OP9 stromal cell-lines (a gift from Dr. Wang Shu's lab at IBN, A*STAR) either seeded on tissue culture 6 well plates (1×10^5 cells/well) under static condition or on microcarriers (2×10^5 cells/20 mg of Solohill microcarriers) in 6 well ULA plates under continuous agitation at 70 rpm. Enucleated cells were enriched by passing through non-woven fabric filters (Tao et al., 2011)(Antoshin, Singapore) or Acrodisc WBC Syringe filters (Pall). Detection of enucleated cells was performed by flow cytometry analysis of live cells stained with 1:100 diluted CD235a-FITC, 1:100 diluted Annexin V and 1:5000 dilution of a cell-permeable nuclear dye, DRAQ-5™ (eBioscience).

RNA extraction and quantitative real-time PCR

Cell samples were lysed in Trizol® reagent (ThermoFisher Scientific) and stored at -80°C until time of RNA extraction. RNA-extraction with DNase-treatment was performed using Direct-zol™ RNA extraction kit (Zymo Research). RNA samples were quantified by O.D260 nm measurements using a NanoDrop UV-Vis spectrophotometer (ThermoFisher Scientific).

500 ng of total RNA was used for 1st strand cDNA synthesis using iScript™ Advanced cDNA synthesis kit (BioRad). cDNA samples diluted 1:10 in RNase-free water were used for quantitative PCR using gene-specific primers (**Table S2**), iTAQ™ Universal SYBR® green supermix (BioRad) and Applied Biosystems® 7500 FAST Real-time PCR system (ThermoFisher Scientific). GAPDH was used as a house-keeping gene for normalization of sample quantities. Relative change in gene expression was determined using the delta-delta c(t) method(Livak et al., 2001).

Immunoblot

Protein extraction, immunoblotting and detection of immunocomplexes were performed as previously detailed (Sivalingam et al., 2018) with the following primary antibodies [1:800 diluted beta-globin (Santa Cruz, SC-21757), 1:400 diluted gamma-globin (Santa Cruz, SC-21756), 1:2000 diluted alpha-globin (Santa Cruz, SC-31110), 1:400 diluted epsilon-globin (Abcam, ab156041) and 1:2000 diluted Actin (Santa Cruz, SC-1615) and relevant secondary antibodies (horse-radish peroxidase (HRP)-conjugated anti-mouse IgG (Jackson ImmunoResearch), HRP-conjugated anti-rabbit IgG (Jackson ImmunoResearch), or HRP-conjugated anti-goat IgG (Jackson ImmunoResearch) at dilution of 1:10000).

Microarray study

Erythroid cells were differentiated from X13-hiPSC according to the method described earlier. Hematopoietic cells from adult peripheral blood from X13 donor were differentiated into erythroid cells by culturing in erythroblast expansion medium for 2 weeks. RNA was extracted from 1 to 2×10^6 cells per sample using Direct-zol RNA MiniPrep Kit (Zymo Research, Irvine, CA). RNA integrity was evaluated using Agilent 2100 Bioanalyzer (Agilent Technologies, Santa Clara, CA) and samples with RNA Integrity Number ≥ 8 were used for expression analysis. Labelled single-stranded cDNA targets were prepared from 250 ng total RNA using the GeneChip WT PLUS Reagent Kit (Life Technologies, Carlsbad, CA) and assayed on the Human Clariom D Array according to manufacturer's protocol. CEL files were extracted from Affymetrix GeneChip Command Console (AGCC) and quality assessment of the CEL files was carried out using Transcriptome Analysis Console (TAC). Raw data from CEL files was RMA-normalized and summarized to transcript clusters using R 'oligo' package. The expression level of genes consisting of multiple transcript clusters was based on the transcript cluster with the highest average expression across samples. Genes with expression value ≥ 6.68 in at least three samples were deemed to be expressed. This threshold was derived from the 95th percentile of background control transcript clusters. Differential gene expression analysis was carried out using Limma. Genes with absolute fold-change ≥ 1.5 and FDR-adjusted p -value < 0.05 (Benjamini-Hochberg method) were deemed as differentially expressed. Volcano plots for comparison between the different groups showing $-\log_{10}$ FDR-adjusted p -value in the y-axis and average \log_2 fold-change in the x-axis were plotted using R. Heat maps of average linkage clustering of gene expression between samples were derived using Heatmapper with Euclidean used for measuring distance between rows and columns (<http://heatmapper.ca/expression/>) (Babicki et al., 2016). Venn diagrams for comparison of DEGs between different groups were done using on-line available tool from VIB-UGent Bioinformatics and Evolutionary Genomics Group (<http://bioinformatics.psb.ugent.be/webtools/Venn/>). Gene ontology of biological processes for DEGs was derived using PANTHER classification system (<http://www.pantherdb.org/>). Gene list for selected categories were derived from Kyoto Encyclopedia of Genes and Genomes (KEGG; <https://www.genome.jp/kegg/>), Gene Ontology resource (<http://geneontology.org/>), Human

MitoCarta 2.0 (<https://www.broadinstitute.org/files/shared/metabolism/mitocarta/human.mitocarta2.0.html>) and Lux et al (Lux et al., 2016). Fold-change in expression of selected DEGs (adult vs hiPSC erythroid cells) specifying important molecular functions was verified by RT-qPCR and compared with microarray data.

Flow cytometry (FACS)

Flow cytometry was performed as previously detailed (Sivalingam et al., 2018) on cells fixed with 4% paraformaldehyde (eBioscience) using NovoCyte Flow cytometer (ACEA Biosciences Inc., USA) and analysed using FlowJo Software. The following antibodies were used for measuring: pluripotency [primary antibodies: 1:100 Oct4 (R&D Systems, USA); 1:50 Tra1-60 (Millipore), 1:100 SSEA4 (BioLegend, USA) and secondary antibody: 1:500 diluted rabbit anti-mouse IgG-FITC conjugate (DAKO)], mesoderm [T-brachyury-FITC (R&D Systems), KDR-PE (Miltenyi Biotec), CD31-PE], hematopoietic marker [CD34-APC, CD43-FITC, CD 45-PE, CD71-APC, CD235a-FITC, CD14-APC, CD15-APC, CXCR4-APC, CD133-FITC (all from BD Biosciences, USA)]. The following antibodies were used as isotype-controls: mouse IgG1-FITC and PE (Miltenyi Biotec, Germany), mouse IgG2b_k-FITC and mouse IgG2a_k-APC (BD Biosciences). For hemoglobin analysis, 0.1% v/v Triton X-100 permeabilized cells were incubated with 1:50 diluted fetal hemoglobin-FITC (ThermoFisher Scientific) or adult hemoglobin-PE antibodies (Santa Cruz Biotechnology, USA). Annexin V staining was performed according to manufacturer's instruction using 1:100 FITC Annexin V antibody (Biolegend). Quantification of fresh normocytes, reticulocytes and erythroblasts were performed by co-staining with Hoescht and Thiazole orange using LSRII Flow Cytometer (BD Biosciences, USA).

Immunohistochemistry and microscope imaging

Cells were cytospun onto glass microscope slides (Marienfeld) using Cytospin™ 4 cytocentrifuge (ThermoFisher Scientific), fixed and stained using Giemsa stain (Sigma-Aldrich) as detailed previously (Sivalingam et al., 2018). Slides were imaged using Axiovert 200M inverted microscope (Zeiss). Immunofluorescence imaging of terminally matured erythroblast was done using Nikon Eclipse Ti-E fluorescence microscope (Nikon). All other cell images were taken using EVOS® Cell imaging system (ThermoFisher Scientific).

Oxygen equilibration curve

Hemox analyzer model B equipment (TCS Scientific Corp) was used to generate the oxygen binding and dissociation equilibration curves of cells as detailed previously (Sivalingam et al., 2018). Adult peripheral blood (donor derived) was run as controls. All samples were measured in duplicates.

Scanning electron microscopy

Electron microscopy was conducted on erythrocytes using the methods outlined in (Malleret et al., 2013).

Quantitative Phase Imaging using Holotomographic Microscopy

HT-2S Tomocube Holotomographic microscope (EINST Technology Pte Ltd) was used to perform 3-D quantitative phase imaging and optical diffraction tomography of single cells. The 3D refractive index (RI) distributions of the erythrocytes were obtained and morphological (cellular volume, surface area, sphericity), biochemical (hemoglobin concentration and content) and mechanical properties (dynamic membrane fluctuation) of RBCs were quantified from the reconstructed 3D RI tomograms using TomoStudio™ software. To obtain properties of the cells, voxels with higher RI than the background were selected. These segmented voxels provided the cell boundary and allowed for calculation of surface area (SA). Number of voxels also corresponded to volume of the entire cell, with cell volume (CV) = No. of voxels of the mask * unit volume. Sphericity was obtained directly from both CV and SA with the equation: Sphericity = $\pi^{1/3} * (6 CV)^{2/3}/SA$.

Cellular Hb concentration (CHC) was calculated based on mean refractive index (RI) of the cell – RI of the medium/ α , where α is a refraction increment of Hb and has a value of 0.2mL/g (Friebel et al., 2006, Park et al., 2009). Cellular Hb (CH) levels were then calculated with CH = CV*CHC*0.01.

The cell membrane fluctuations were obtained by first generating the 2D membrane fluctuation map which is defined as the temporal standard deviation of mean cell height profiles for the RBCs. The spatial average of this 2D membrane fluctuation map over the projected cell area provided the measure of membrane fluctuation (Lee et al., 2017, Park et al., 2016).

Statistical analysis

Statistical analysis was performed using GraphPad Prism 6 (GraphPad Software Inc.). Student's unpaired *t*-test was used for comparison between two groups with equal variance and the Mann-Whitney test was used when variances were not assumed to be equal. One-way ANOVA was used for multiple groups (more than 2 groups) comparison. Statistical tests were performed on the pooled data from at least 3 independent replicates. *P* values < 0.05 were considered significant. **p* < 0.05, ***p* < 0.01, ****p* < 0.001.